
Forced Resonance Orbit Analysis of Binary Asteroid System Orbit with Consideration of Solar Radiation Pressure

Ying-Jing Qian^{1*}, Kai Zong¹, Xiao-Dong Yang¹, Zhen Si², Feng Gao³

¹ Beijing Key Laboratory of Nonlinear Vibrations and Strength of Mechanical Structures, Beijing University of Technology, Beijing 100124, P. R. China

² Nuclear Equipment Safety and Reliability Center, China Academy of Machinery Science and Technology, Beijing 100044, P. R. China

³ School of Astronautics, Harbin Institute of Technology, Harbin 150001, P. R. China

Abstract: The solar radiation pressure becomes one of the major perturbations to orbits in the study of binary asteroid system, since asteroids have relatively weak gravity fields. In this paper, based on the idea of treating the solar radiation pressure as periodic external excitation, one novel family of orbits due to primary resonance and another novel family of orbits due to both primary resonance and internal resonance have been found by the classical perturbation method. The two types of steady-state orbits due to external resonance with different area-to-mass ratios have been determined and discussed by the frequency-response equations. Five binary asteroid systems, 283 Emma-S/2003 (283) 1, 22 Kalliope-Linus, 31 Euphrosyne-S/2019 (31) 1, 2006 Polonskaya-S/2005 (2006) 1 and 4029 Bridges have been taken as examples to show the validity of the proposed mechanism in the explanation of orbits formation due to resonance.

Keywords: Binary Asteroid System; Solar Radiation Pressure; Resonance Orbit; Primary resonance; Internal resonance; Nonlinear Analysis

* Corresponding authors: Y.-J. Qian (candiceqyj@163.com), Fax:+86-10-67391617;

1 INTRODUCTION

Over the recent years, the space exploration community has developed a significant interest in asteroid systems. Missions to asteroids are now an important component of space explorations. Some well-known missions include Dawn mission (successfully flew around Ceres and Vesta)[1], NEAR Shoemaker (orbited around 433Eros and became the first of its kind to soft-land on it)[2], JAXA's Hayabusa (landed on the Itokawa in 2005)[3] and Hayabusa-2 mission(planned to return samples from the 1999 JU3)[4]. Among the total asteroid population, the binary asteroid system (BAS) accounts for approximately 15% of the near-Earth asteroids population with a diameter greater than 200m[5; 6]. The binary asteroid system was confirmed to exist by the Galileo spacecraft when it flies by the Ida-Dactyl system[7]. Till now, missions around the binary asteroid systems are still in the planning stage, such as ESA's Marco Polo-R mission[8] and NASA and ESA's cooperation project AIDA[9]. Those missions can enrich our knowledge on the physics of small bodies and push the exploration of the history about our solar system.

Since asteroids in the solar system have smaller mass than the planets and dwarf planets, the asteroids' own gravitational force is generally weak. Correspondingly, the environmental perturbations including solar gravitational perturbation, gravitational perturbation from other large bodies and solar radiation pressure (SRP) might have non-negligible influence to orbits around asteroids. Taking the spacecraft with average area-to-

mass ratio $0.02m^2/kg$ as an example, when the spacecraft enters the main belt asteroid 216 Kleopatra's Hill radius, the gravity of the asteroid itself is about 10^{-3} magnitude, the SRP perturbation is about 10^{-6} magnitude, the solar gravitational perturbation is 10^{-9} magnitude, and the gravitational perturbation from other large bodies is about 10^{-15} magnitude[10]. In such condition, the solar radiation pressure is the main source of perturbation which should be considered.

Literatures pay great attention to the effects of SRP perturbation acting on the orbit stability and bifurcations for asteroid systems[11]. Hamilton et al.[12] pointed out that the SRP can cause large oscillations of the spacecraft's orbital eccentricity and semi-major axis. Feng and Hou[13] also mentioned that for smaller asteroids with sizes on the order of a few kilometers or less, the SRP can cause the spacecraft to escape or impact on the small body. Alessi[14] showed that the importance of some resonances caused by SRP in low earth orbits. Yáñez et al.[15] studied the influence of SRP on the linear stability of planar symmetric periodic orbits around minor bodies. Chanut et al.[16] analyzed the stabilities of the equatorial orbits of asteroid (101955) Bennu due to effects of SRP.

Aforementioned literatures illustrated the great influence of the SRP on the orbital stability and bifurcations, and showed the orbits sensitivity to initial conditions due to the SRP. However, by the powerful numerical correction method and continuation methods, three types of orbits still can be found by utilizing SRP as part of the system. The first type of orbit is the circum-asteroid periodic orbits under SRP obtained in the Hill model

including the retrograde and prograde orbits, such as the orbiting trajectories about various sized asteroids found by Morrow et al.[17]. Another type of orbit is the powered hovering orbits around asteroids. Xin [18] found forced-oscillation hovering motions in the vicinity of equilibrium points due to SRP by adopting a triaxial ellipsoid model for the asteroid. Broschart and Scheeres[19] and Sawai et al.[20] presented the hovering orbits above asteroid (25143) Itokawa by a nearly continuous control thrust. Mysen and Aksnes[21] explored the stability boundary created by the rotation of the Rosetta orbiter exposed by radiation from the Sun. Takei et.al[22] applied planer model of SRP to Hayabusa2's station-keeping operation in the proximity of the asteroid Ryugu. The station-keeping process is similar to the one done by Scantamburlo and Guzzo [23]. The last type of orbit involves the Sun-terminator orbit[24], quasi-terminator orbit[25] and its alternating orbit near the asteroid utilizing the solar sail spacecraft[26-28].

Especially, for the binary asteroid system, it is suggested that, from an engineering point of view, a spacecraft would have a greater advantage in a hovering motion than in an orbital motion [29]. Heiligers and Scheeres[30] studied the utilization of SRP on a solar sail to generate artificial equilibrium points and hovering periodic orbits for asteroid mission. De Almeida, AK, Jr et.al [31] determine the locations of artificial equilibrium point considering the spacecraft with thrust such as planar solar sails, which makes possible the observation of the poles of the components of the binary system. Hou[32] studied a type of hovering orbit named forced-oscillation motion with two tri-axial ellipsoids for the

asteroid systems. Utilizing the polyhedral shape to accurately model the gravitational field, Aljbaae et al.[33] provided a generalized discussion on the dynamics of a spacecraft around the binary asteroid system, (90) Antiope, under the influence of solar radiation pressure. Jean et al.[34] compared the influence of different SRP acceleration models acting on the spacecraft near a binary asteroid.

It is noted that most literatures focused on the effects of the SRP on the orbital elements[12] and the correction algorithms to obtain the final orbit solutions with linear solutions as initial guesses[32; 35; 36]. Some stability analyses have been conducted by numerically computing eigenvalues of monodromy matrix [37; 38]. Other stability analyses are done by checking whether the designated threshold (eccentricity or other parameters) is exceeded[16; 39; 40]. However, the contributions from the system's nonlinearity, which may cause energy transferring and frequency varying under the influence of SRP, have not been reported yet. Hence, it is essential to understand the mechanism of one periodic orbit from the view point of varying frequency due to SRP. One of the best options may be to evaluate the orbits and their stability by a macroscopic analytical technique.

Since the SRP can be considered as perturbation[41] to the binary asteroid system, the perturbation techniques[42] may effectively treat those questions. The perturbation methods originate from celestial mechanics to study weak gravitational influences, which have been used in mechanical vibration field in recent years. From the perspective of the

nonlinear oscillations theory, it can be found that, due to the approximate periodic motion between the Sun and the binary asteroid system, the SRP appears as periodic external excitation in the dynamic equation[43], in which the SRP mathematically leads to non-homogeneous dynamic equations. It is worthy to mention that, with certain parameters, the external excitation system has stable periodic orbit solutions due to the resonance[42]. In other words, the SRP excitation can be used to create stable orbits.

According to the literatures[42; 44], the possible primary resonance occurs when the external periodic excited frequency ω is close to the system's natural frequencies ω_n ($n=1,2,3$), and the superharmonic/subharmonic resonance occurs when the external excitation frequency is equal to several times of the natural frequencies. Therefore, the asteroid systems are highly possible for resonance, as long as the its n th order natural frequency ω_n and the SRP excitation frequency Ω satisfies the relations that $\Omega=N\omega_n$ or $\Omega=\omega_n/N$ (N is an integer real number), resonance can occur. In addition, due to the contributions of nonlinearity, the possibilities for resonance can be further expanded to $\Omega=N\omega_n+\sigma$ or $\Omega=\omega_n/N+\sigma$ (σ is detuning parameter) through slowly changes in amplitudes and phases[42]. Those abundant resonance conditions provide new opportunities to design the periodic orbit families for asteroid exploration. We will analyze the Long/short period motion frequencies and the SRP frequency for some real binary asteroid systems, which is listed in Table 1. It can be found that the primary resonance condition fits all the systems in Table 1 that SRP frequency ω is approximately equal to the in-plane short-period motion ω_2 . In

addition, many systems have 1:3 internal resonances (Detailed information can be found in Section 2). The nonlinear oscillations theory provides a new way for mathematically explaining the analytical expressions of the periodic orbits and exploring the contributions of nonlinearity, which needs to be further studied.

The remainder of this paper is structured as follows. In Section 2, the BAS-Sun-spacecraft system is introduced in detail. During the derivation, the BAS-Spacecraft model is considered as circular restricted three-body problem (CRTBP) with SRP taken into account since the Sun rotates clockwise around the barycenter in the same plane. By analyzing the natural frequencies of BASs and SRP external excitation frequency, two cases of forced resonance orbits are considered in Section 3 by the classical perturbation method. The numerical simulations and interesting nonlinear dynamical behaviors including jumping phenomenon and energy transferring from short period motion to the long period motion are investigated in Section 4. The conclusions are drawn in Section 5.

2 DYNAMIC MODEL

Binary asteroid systems are composed of two bodies orbiting their barycenter. In the present studies, the two asteroids and spacecraft system are considered as CRTBP: two primaries are assumed to revolve around their barycenter in circular orbits under their mutual gravitational attractions. The small spacecraft is “massless”, which is attracted by the two primaries and moves in the plane defined by the two primaries. We assume that the

motions of the primary bodies are not affected by the particle. The modeling problem becomes more complicated when non-spherical terms of the asteroids are considered. In this study, we focus on systems that fit the CRTBP assumption which are nearly sphere-restricted synchronous systems or rotationally symmetric asteroids with their equatorial planes coinciding with their mutual orbit plane.

The geometry of the BAS-Spacecraft-Sun problem is conveniently described in a synodic coordinate system ($o-xyz$), which is centered at the barycenter of the two primaries O , as shown in Fig.1(a). The m_1 represents the mass of the larger primary and m_2 represents the mass of the smaller one. Ω is the angular speed of the BAS. R_1 and R_2 are the distance of the particle from the larger primary and the smaller one, respectively. L denotes the distance of two primaries. m_s is the mass of the Sun. R denotes the distance between barycenter O and spacecraft, R_{so} is the distance between barycenter O and Sun. θ is the angle between the Sun light and the x -axis.

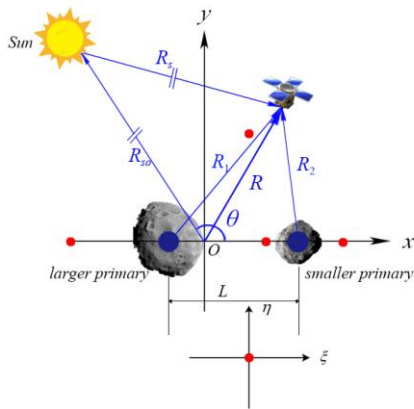


Figure 1(a) Geometry of BAS-Sun-Spacecraft System in x - y plane

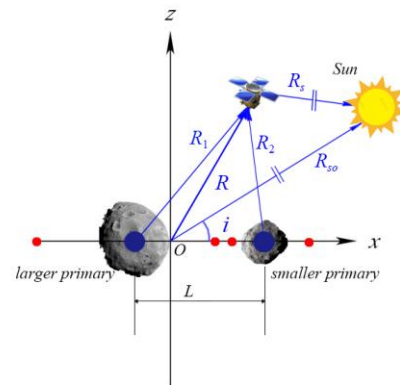


Figure 1(b) Geometry of BAS-Sun-Spacecraft System in x - z plane

We assume that the Sun rotates clockwise in a circular orbit around the barycenter with a constant inclination i , as shown in Fig.1(b). At the initial time, the Sun is assumed to be on the positive x axis. The distance between the Sun and the center of the BAS maintains a constant. Since the magnitude of solar gravitational perturbation is two orders lower than that of SRP, only the SRP is considered during the modeling, which appears as an inhomogeneous term in the synodic system.

Since $R/R_{so} \ll 1$, the periodic external excitation of the Sun in x - y plane can be approximately expressed as

$$\mathbf{F}_{SRP} = \frac{\beta_{\odot}}{R_{so}^2} [-\cos i \cos \theta \quad -\cos i \sin \theta]^T \quad (1)$$

where

$$\beta_{\odot} = (1 + \alpha) W_o R_o^2 \frac{S}{M} \quad (2)$$

in which α is the reflection coefficient, $W_o = 4.56 \mu N m^{-2}$ is the solar pressure at $R_o = 1 \text{ AU}$, and S/M is the effective area-to-mass ratio of the spacecraft.

We define $\mu = m_2 / (m_1 + m_2)$ as the mass parameter of the system and consider the distance L of two primaries as the unit. So, the larger primary, with a mass of $1 - \mu$, is located at $(-\mu, 0, 0)$; the smaller one, with a mass of μ , is located at $(1 - \mu, 0, 0)$, and the mass of the Sun is $\mu_s = m_s / (m_1 + m_2)$. In this synodic coordinate system, the time unit is defined as the period time of the smaller primary around the larger one. The non-dimensional equation of motion for spacecraft's is obtained as

$$\begin{aligned}\ddot{x} - 2\dot{y} &= \frac{\partial V}{\partial x} - F \cos(\omega t) \\ \ddot{y} + 2\dot{x} &= \frac{\partial V}{\partial y} - F \sin(\omega t)\end{aligned}\tag{3}$$

where the nondimensional SRP acceleration $F = (\beta_\theta / R_{so}^2) \cos i / (\Omega^2 L)$, and the angular rate of the Sun line in the synodic coordinate system can be expressed as

$$\omega = 1 - \sqrt{\mu_s / r_{so}^3}\tag{4}$$

in which $r_{so} = R_{so} / L$, $\mu_s = m_s / (m_1 + m_2)$. The pseudo-potential function V of the system is given by

$$V = \frac{x^2 + y^2}{2} + \frac{1 - \mu}{r_1} + \frac{\mu}{r_2}\tag{5}$$

in which r_1 and r_2 are the nondimensional distances of the particle from the larger primary and the smaller one, respectively. Note that the SRP is considered as external excitation and does not affect the system's natural frequencies and the equilibrium points. Without considering SRP, the unperturbed part is the classical CRTBP. In such system, equilibrium points in the synodic frame still exist.

To investigate the motion around the equilibrium points of the BAS, it is necessary to move the origin of the coordinate system from the barycenter of the system to the equilibrium point. We take the triangular equilibrium point L_4 as an example, the relationship between the new coordinate system $L_4\text{-}\xi\eta\zeta$ and the synodic coordinate system $(o\text{-}xyz)$ can be expressed as

$$(\xi, \eta, \zeta)^T = (x - x_o, y - y_o, z)^T / \gamma_o\tag{6}$$

where x_o and y_o are the coordinate of the equilibrium point, γ_o is the unit of length rescaled as the distance between the equilibrium point and its closest primary.

The pseudo-potential function of the motion around the L_4 point could be expressed with the Legendre polynomials P_n . By this way, Equation (3) can be rewritten as

$$\begin{aligned}\ddot{\xi} - 2\dot{\eta} - V_{\xi\xi}\xi - V_{\xi\eta}\eta &= \sum_{n=2}^{\infty} \sum_{\substack{i+j+k=n, \\ i,j,k \in N}} \alpha_{ijk} \xi^i \eta^j \zeta^k - F \cos(\omega t) \\ \ddot{\eta} + 2\dot{\xi} - V_{\xi\eta}\xi - V_{\eta\eta}\eta &= \sum_{n=2}^{\infty} \sum_{\substack{i+j+k=n, \\ i,j,k \in N}} \beta_{ijk} \xi^i \eta^j \zeta^k - F \sin(\omega t)\end{aligned}\tag{7}$$

where $V_{\xi\xi}=3/4$, $V_{\eta\eta}=9/4$, $V_{\xi\eta}=\frac{3\sqrt{3}}{4}(1-2\mu)$, and α_{ijk} , β_{ijk} are known constants. The expressions up to third order can be found in the Appendix as A2.

By solving the eigen problem of the linear part of Equation (7), the natural frequencies for the motions around the L_4 point can be obtained. By Equation (4), the frequency of SRP in different BASs also can be obtained. Twelve BASs are taken as examples, and the natural frequencies and the corresponding SRP frequencies are listed in Table 1.

Table 1 Long/short period motion frequencies and the SRP frequencies for some BASs

Binary Asteroid System	μ	Long period motion frequency (ω_1)	Short period motion frequency (ω_2)	Frequency of SRP (ω)
31 Euphrosyne-S/2019(31) 1	0.000016	0.01032790	0.99994666	0.99923270
121 Hermione-S/2002(121) 1	0.004986	0.18625610	0.98250122	0.99938936
624Hektor-Skamandrios	0.000277	0.04329963	0.99906213	0.99964569
2006 Polonskaya-S/2005 (2006) 1	0.010471	0.27500933	0.96144155	0.99938818

7088 Ishtar-unnamed	0.017651	0.36788415	0.92987162	0.99916322
283 Emma-S/2003(283) 1	0.000298	0.04490272	0.99899136	0.99785612
1866 Sisyphus-Secondary	0.000985	0.08176847	0.99665135	0.99890915
379 Huenna-S/2003(379) 1	0.000291	0.04439217	0.99901418	0.95102605
1990TR-Secondary	0.005713	0.19983568	0.97982942	0.99929691
4029 Bridges-Secondary	0.013592	0.31721890	0.94835234	0.99955159
22 Kalliope-Linus	0.004776	0.18216969	0.98326710	0.99800815

Generally, for a two-dimensional system, there are two natural frequencies ω_1 and ω_2 (assuming that $\omega_2 > \omega_1$) denoting respectively the long and the short period orbits. In [Table 1](#), it can be found that the second natural frequency ω_2 of most BAS is very close to frequencies of SRP ω , that $\omega \approx \omega_2$. It is known that the possible resonance occurs when the external periodic excited frequency is close to the system's natural frequency. Thus, the second primary resonance phenomena may occur for all the systems in [Table 1](#). In addition, some BASs' second natural frequencies are around the three times of the first natural frequency, that $\omega_2 \approx 3\omega_1$. Hence, 1:3 internal resonances are also possible for these BAS, such as 4029 Bridges-Secondary, 2006 Polonskaya-S/2005 (2006) 1 and 7088 Ishtar-unnamed.

3 FORCED RESONANCE ORBIT ANALYSIS

In this section, two cases are investigated. In Case I, only the second primary resonance is considered. In Case II, both the second primary resonance and 1:3 internal resonance between the long period and short period motions are taken into consideration

to find the forced resonance orbits. Generally, the 1:3 internal resonance affects the final orbits of the system through the cubic nonlinear terms. We truncate the Equation (7) into third order. By utilizing the method of multiple scales, an approximation of the system can be obtained and the stability for steady-state motions is analyzed, which will further benefit the trajectory design in asteroid missions.

We seek an asymptotic solution to Equation (7) in the form

$$\begin{aligned}\xi &= \varepsilon \xi_1(T_0, T_2) + \varepsilon^2 \xi_2(T_0, T_2) + \varepsilon^3 \xi_3(T_0, T_2) \\ \eta &= \varepsilon \eta_1(T_0, T_2) + \varepsilon^2 \eta_2(T_0, T_2) + \varepsilon^3 \eta_3(T_0, T_2)\end{aligned}\quad (8)$$

where the $T_0=t$, is a fast time scale, $T_2=\varepsilon^2 t$, is a slow time scale, and ε is a bookkeeping device to denote following small terms.

Then, the derivatives with respect to t become expansions in terms of the partial derivatives with respect to the T_n according to

$$\begin{aligned}\frac{d}{dt} &= \frac{\partial}{\partial T_0} \frac{dT_0}{dt} + \frac{\partial}{\partial T_2} \frac{dT_2}{dt} = D_0 + \varepsilon^2 D_2 \\ \frac{d^2}{dt^2} &= \frac{\partial}{\partial T_0} (D_0 + \varepsilon^2 D_2) \frac{dT_0}{dt} + \frac{\partial}{\partial T_2} (D_0 + \varepsilon^2 D_2) \frac{dT_2}{dt} = D_0^2 + 2\varepsilon^2 D_0 D_2\end{aligned}\quad (9)$$

Here only the terms of order ε^2 are keep and higher order terms are truncated.

Moreover, we set F in Equation (7) equals to $\varepsilon^3 f$. So that the effect of nonlinearity and excitation will appear in the same perturbation equations. Then, substituting Equation (8) and Equation (9) into Equation (7) and equating coefficient of ε , we obtain:

Order ε^1

$$\begin{cases} D_0^2 \xi_1 - 2D_0 \eta_1 - V_{\xi\xi} \xi_1 - V_{\xi\eta} \eta_1 = 0 \\ D_0^2 \eta_1 + 2D_0 \xi_1 - V_{\xi\eta} \xi_1 - V_{\eta\eta} \eta_1 = 0 \end{cases} \quad (10)$$

Order ε^2

$$\begin{cases} D_0^2 \xi_2 - 2D_0 \eta_2 - V_{\xi\xi} \xi_2 - V_{\xi\eta} \eta_2 = \alpha_{200} \xi_1^2 + \alpha_{110} \xi_1 \eta_1 + \alpha_{020} \eta_1^2 \\ D_0^2 \eta_2 + 2D_0 \xi_2 - V_{\xi\eta} \xi_2 - V_{\eta\eta} \eta_2 = \beta_{200} \xi_1^2 + \beta_{110} \xi_1 \eta_1 + \beta_{020} \eta_1^2 \end{cases} \quad (11)$$

Order ε^3

$$\begin{cases} D_0^2 \xi_3 - 2D_0 \eta_3 - V_{\xi\xi} \xi_3 - V_{\xi\eta} \eta_3 = 2D_2 \eta_1 - 2D_0 D_2 \xi_1 + \alpha_{030} \eta_1^3 + \alpha_{120} \eta_1^2 \xi_1 \\ \quad + \alpha_{210} \xi_1^2 \eta_1 + \alpha_{300} \xi_1^3 + 2\alpha_{200} \xi_1 \xi_2 + \alpha_{110} (\xi_1 \eta_2 + \xi_2 \eta_1) + 2\alpha_{020} \eta_1 \eta_2 - f \cos \omega t \\ D_0^2 \eta_3 + 2D_0 \xi_3 - V_{\xi\eta} \xi_3 - V_{\eta\eta} \eta_3 = -2D_0 D_2 \eta_1 - 2D_2 \xi_1 + \beta_{030} \eta_1^3 + \beta_{120} \eta_1^2 \xi_1 \\ \quad + \beta_{210} \xi_1^2 \eta_1 + \beta_{300} \xi_1^3 + 2\beta_{200} \xi_1 \xi_2 + \beta_{110} (\xi_1 \eta_2 + \xi_2 \eta_1) + 2\beta_{020} \eta_1 \eta_2 - f \sin \omega t \end{cases} \quad (12)$$

The solution to Equation (10) can be easily obtained as:

$$\begin{aligned} \xi_1 &= A_1(T_2) e^{i\omega_1 T_0} + A_2(T_2) e^{i\omega_2 T_0} + cc \\ \eta_1 &= \Gamma_1 A_1(T_2) e^{i\omega_1 T_0} + \Gamma_2 A_2(T_2) e^{i\omega_2 T_0} + cc \end{aligned} \quad (13)$$

where cc denotes the complex conjugates of all preceding terms of the right-hand side and

$$\Gamma_r = \frac{2i\omega_r - V_{\xi\eta}}{\omega_r^2 + V_{\eta\eta}} = \frac{-V_{\xi\xi} - \omega_r^2}{2i\omega_r + V_{\xi\eta}}, (r = 1, 2) \quad (14)$$

3.1 CASE I: SECOND PRIMARY RESONANCE $\omega \approx \omega_2$

The second primary resonance is considered in this section. The detuning parameter τ is introduced and denoted as

$$\omega = \omega_2 + \varepsilon^2 \tau \quad (15)$$

Substituting Equation (13) to Equation (11), we could obtain the solutions of ξ_2 and η_2 in Equation (11). Then, employing the Euler's formula and substituting ξ_1 and η_1 , ξ_2

and η_2 into Equation (12), we obtain

$$\begin{aligned}
D_0^2 \xi_3 - 2D_0 \eta_3 - V_{\xi\xi} \xi_3 - V_{\xi\eta} \eta_3 &= (2\Gamma_1 - 2i\omega_1) D_2 A_1 e^{i\omega_1 T_0} + (2\Gamma_2 - 2i\omega_2) D_2 A_2 e^{i\omega_2 T_0} \\
&\quad + U_1 e^{i\omega_1 T_0} + U_2 e^{i\omega_2 T_0} - \frac{1}{2} f e^{i\omega_2 T_0} e^{i\tau T_2} + \dots + cc \\
D_0^2 \eta_3 + 2D_0 \xi_3 - V_{\xi\eta} \xi_3 - V_{\eta\eta} \eta_3 &= (-2\Gamma_1 i\omega_1 - 2) D_2 A_1 e^{i\omega_1 T_0} - (2\Gamma_2 i\omega_2 + 2) D_2 A_2 e^{i\omega_2 T_0} \\
&\quad + V_1 e^{i\omega_1 T_0} + V_2 e^{i\omega_2 T_0} + \frac{i}{2} f e^{i\omega_2 T_0} e^{i\tau T_2} + \dots + cc
\end{aligned} \tag{16}$$

where the terms starting with U_1 , U_2 , V_1 , V_2 obviously can result in secular terms, and the expressions of which can be found in the Appendix as Equation A3.

To determine the solvability conditions of Equation (16), we seek a particular solution in the form

$$\begin{aligned}
\xi_3 &= P_1 e^{i\omega_1 T_0} + Q_1 e^{i\omega_2 T_0} \\
\eta_3 &= P_2 e^{i\omega_1 T_0} + Q_2 e^{i\omega_2 T_0}
\end{aligned} \tag{17}$$

Substituting Equation (17) into Equation (16), and equating the coefficients of $\exp(i\omega_1 T_0)$ and $\exp(i\omega_2 T_0)$ on both side, we obtain

$$\begin{cases}
-(\omega_1^2 + V_{\xi\xi}) P_1 - (2i\omega_1 + V_{\xi\eta}) P_2 = X_{11} \\
-(\omega_2^2 + V_{\xi\xi}) Q_1 - (2i\omega_2 + V_{\xi\eta}) Q_2 = X_{12} \\
(2i\omega_1 - V_{\xi\eta}) P_1 - (\omega_1^2 + V_{\eta\eta}) P_2 = Y_{11} \\
(2i\omega_2 - V_{\xi\eta}) Q_1 - (\omega_2^2 + V_{\eta\eta}) Q_2 = Y_{12}
\end{cases} \tag{18}$$

where

$$\begin{aligned}
X_{11} &= (2\Gamma_1 - 2i\omega_1) D_2 A_1 + U_1 \\
X_{12} &= (2\Gamma_2 - 2i\omega_2) D_2 A_2 + U_2 - 0.5 f e^{i\tau T_2} \\
Y_{11} &= (-2\Gamma_1 i\omega_1 - 2) D_2 A_1 + V_1 \\
Y_{12} &= -(2\Gamma_2 i\omega_2 + 2) D_2 A_2 + V_2 + 0.5 i f e^{i\tau T_2}
\end{aligned} \tag{19}$$

Thus, the problem of determining the solvability conditions of Equation (16) is reduced to that of determining the solvability conditions of Equation (18):

$$\begin{vmatrix} -\omega_1^2 - V_{\xi\xi} & X_{11} \\ 2i\omega_1 - V_{\xi\eta} & Y_{11} \end{vmatrix} = 0 \quad \begin{vmatrix} -\omega_2^2 - V_{\xi\xi} & X_{12} \\ 2i\omega_2 - V_{\xi\eta} & Y_{12} \end{vmatrix} = 0 \quad (20)$$

Substituting Equation (19) into Equation (20) we obtain

$$\begin{aligned} D_2 A_1 &= i\Lambda_1 \left[G_{11} A_1 A_2 \bar{A}_2 + G_{12} A_1^2 \bar{A}_1 \right] \\ D_2 A_2 &= i\Lambda_2 \left(G_{21} A_1 A_2 \bar{A}_1 + G_{22} A_2^2 \bar{A}_2 + 0.5(\bar{\Gamma}_2 i - 1) f e^{iT_2} \right) \end{aligned} \quad (21)$$

where

$$\Lambda_r = \frac{\omega_r^2 + V_{\eta\eta}}{2\omega_r (4 - V_{\xi\xi} - 2\omega_r^2 - V_{\eta\eta})}, \quad r = 1, 2 \quad (22)$$

Since G_{11} , G_{12} , G_{21} , and G_{22} are all complex, we express them as $G_{11}=R_{11}+iI_{11}$, $G_{12}=R_{12}+iI_{12}$, $G_{21}=R_{21}+iI_{21}$, $G_{22}=R_{22}+iI_{22}$. The R_{11} , I_{11} , R_{12} , I_{12} , R_{21} , I_{21} , R_{22} , I_{22} are all real functions of nonlinear terms in Equation (7). The expressions of them are shown in Appendix as A4.

Note that A_1 and A_2 are considered as functions of the slow time T_2 and the complex amplitude A_n can be expressed as $A_n=0.5a_n \exp(i\beta_n)$ with real a_n and β_n . By introducing the $\varphi_1=\beta_1$, $\varphi_2=\tau T_2-\beta_2$, the real and imaginary parts of Equation (21) can be separated as

$$\begin{aligned} D_2 a_1 &= -\Lambda_1 I_{11} \frac{a_1 a_2^2}{4} - \Lambda_1 I_{12} \frac{a_1^3}{4} \\ a_1 D_2 \varphi_1 &= \Lambda_1 R_{11} \frac{a_1 a_2^2}{4} + \Lambda_1 R_{12} \frac{a_1^3}{4} \\ D_2 a_2 &= -\Lambda_2 I_{21} \frac{a_1^2 a_2}{4} - \Lambda_2 I_{22} \frac{a_2^3}{4} - 2\Lambda_2 R_{23} \sin \varphi_2 - 2\Lambda_2 I_{23} \cos \varphi_2 \\ a_2 D_2 \varphi_2 &= -\Lambda_2 R_{21} \frac{a_1^2 a_2}{4} - \Lambda_2 R_{22} \frac{a_2^3}{4} - 2\Lambda_2 R_{23} \cos \varphi_2 + 2\Lambda_2 I_{23} \sin \varphi_2 + a_2 \tau \end{aligned} \quad (23)$$

Therefore, the first-order approximation for the general solution Equation (13) is

$$\begin{aligned}\xi_1 &= 0.5a_1e^{i(\omega_1T_0+\varphi_1)} + 0.5a_2e^{i(\omega_1T_0-\varphi_2)} + cc \\ \eta_1 &= \Gamma_1 0.5a_1e^{i(\omega_1T_0+\varphi_1)} + \Gamma_2 0.5a_2e^{i(\omega_1T_0-\varphi_2)} + cc\end{aligned}\quad (24)$$

Note, Equation (24) is the first-order approximation of the system instead of a linear solution. Affected by the system's nonlinearity, the variations of a_n , and φ_n ($n = 1, 2$) in Equation (24) strictly follow Equation (23). However, the amplitudes of the linear solution can be chosen as any value.

It is known that steady-state motions occur when $D_2a_1=D_2a_2=0$, $D_2\varphi_1=D_2\varphi_2=0$, which corresponds to the singular points of Equation (23). It is clear that $a_1=0$ must be the steady-state motion for the long period motion (i.e., motion relevant to ω_1). For the steady-state motion, the short period motion (i.e., motion relevant to ω_2) must be

$$\begin{aligned}D_2a_{20} &= -\Lambda_2 I_{22} \frac{a_{20}^3}{4} + \Lambda_2 f \sin \varphi_{20} - \Lambda_2 \bar{\Gamma}_2 f \cos \varphi_{20} \\ a_{20} D_2\varphi_{20} &= -\Lambda_2 R_{22} \frac{a_{20}^3}{4} + \Lambda_2 f \cos \varphi_{20} + \Lambda_2 \bar{\Gamma}_2 f \sin \varphi_{20} + a_{20} \tau\end{aligned}\quad (25)$$

where the subscript 0 denotes steady-state values. Then, Equation (25) can be rewritten as

$$16\Lambda_2^2 f^2 (1 + \bar{\Gamma}_2^2) = 16a_{20}^2 \tau^2 + a_{20}^6 \Lambda_2^2 (R_{22}^2 + I_{22}^2) - 8a_{20}^4 \Lambda_2 R_{22} \tau \quad (26)$$

which is named as *frequency-response equation* or *amplitude of the excitation-amplitude of response equation*. Here we express the steady-state amplitude of the response a_{20} as function of detuning parameter τ and solar radiation force f . It is clear that once the detuning parameter τ ($\tau=\omega-\omega_2$) and system parameters are given, the amplitude of the response a_{20} is determined. Then, the steady-state phase of the response φ_{20} could be solved by Equation (25).

However, it is possible for one detuning parameter τ to result in two or three values of steady-state amplitude solutions a_{20} by Equation (26). It is necessary to evaluate the stability of the steady-state solutions. One simple way is to investigate the nature of the singular points of Equation (25). The Jacobi matrix of Equation (25) can be obtained as

$$A = \begin{bmatrix} -\Lambda_2 I_{22} \frac{3a_{20}^2}{4} & a_{20} \tau - \Lambda_2 R_{22} \frac{a_{20}^3}{4} \\ -\tau + \Lambda_2 R_{22} \frac{3a_{20}^2}{4} & \Lambda_2 I_{22} \frac{a_{20}^3}{4} \end{bmatrix} \quad (27)$$

Let p is the trace of $[A]$ and q is the determinant of $[A]$, we obtain the eigenvalues of $[A]$

$$\lambda_{1,2} = \frac{1}{2} p \mp \left(\frac{1}{4} p^2 - q \right)^{1/2}, \quad (28)$$

when λ is a pure imaginary number or has negative real part, the solution is stable.

By employing the Euler's formula, the first-order approximation to the forced resonance orbit is found as

$$\begin{aligned} \xi &= a_{20} \cos(\omega t - \varphi_{20}), \\ \eta &= \Gamma_2 a_{20} \cos(\omega t - \varphi_{20}). \end{aligned} \quad (29)$$

3.2 CASE II: SECOND PRIMARY RESONANCE WITH CONSIDERATION OF 1:3

INTERNAL RESONANCE $\omega \approx \omega_2$, $\omega_2 \approx 3\omega_1$

In this subsection, we restrict our attention to the case with 1:3 internal resonance. In the presence of internal resonance, the steady-state motions become coupled and more complicated. In addition to the detuning parameter τ in Equation (15), we introduce the

second detuning parameter σ representing the deviation between $3\omega_1$ and ω_2 ,

$$\omega_2 = 3\omega_1 + \varepsilon^2 \sigma, \quad (30)$$

and express $(\omega_2 - 2\omega_1)T_0$ as $(\omega_2 - 2\omega_1)T_0 = \omega_1 T_0 + \sigma T_2$, then, [Equation \(16\)](#) can be rewritten as

$$\begin{aligned} D_0^2 \xi_3 - 2D_0 \eta_3 - V_{\xi\xi}^o \xi_3 - V_{\xi\eta}^o \eta_3 &= (2\Gamma_1 - 2i\omega_1) D_2 A_1 e^{i\omega_1 T_0} + (2\Gamma_2 - 2i\omega_2) D_2 A_2 e^{i\omega_2 T_0} \\ &+ U_1' e^{i\omega_1 T_0} + U_2' e^{i\omega_2 T_0} + \frac{1}{2} f e^{i\omega_2 T_0} e^{i\tau T_2} + \dots + cc \\ D_0^2 \eta_3 + 2D_0 \xi_3 - V_{\xi\eta}^o \xi_3 - V_{\eta\eta}^o \eta_3 &= (-2\Gamma_1 i\omega_1 - 2) D_2 A_1 e^{i\omega_1 T_0} - (2\Gamma_2 i\omega_2 + 2) D_2 A_2 e^{i\omega_2 T_0} \\ &+ V_1' e^{i\omega_1 T_0} + V_2' e^{i\omega_2 T_0} + \frac{i}{2} f e^{i\omega_2 T_0} e^{i\tau T_2} + \dots + cc \end{aligned} \quad (31)$$

Since the internal resonance affects the process of merging secular terms, the U_1, U_2, V_1, V_2 are functions of system's nonlinear coefficients that are different from U_1, U_2, V_1, V_2 in [Equation \(16\)](#). The expressions for U_1, U_2, V_1, V_2 can be found in the Appendix as A5.

Similar to the process of [Equation \(17\)](#)-[Equation \(22\)](#), by introducing $\varphi_1 = \beta_1 + \sigma T_2 - 3\beta_1$, $\varphi_2 = \tau T_2 - \beta_2$, and introducing the polar notation A_n as $0.5a_n \exp(i\beta_n)$, the real and imaginary parts of [Equation \(31\)](#) can be separated. A set of time-dependent equations that govern the time variation of the amplitudes and phases can be derived as

$$\begin{aligned} D_2 a_1 = f_1 &= -\frac{1}{4} \Lambda_1 I_{11}' a_1 a_2^2 - \frac{1}{4} \Lambda_1 I_{12}' a_1^3 - \frac{1}{4} \Lambda_1 a_1^2 a_2 \left(R_{13}' \sin \varphi_1 + I_{13}' \cos \varphi_1 \right) \\ D_2 \varphi_1 = f_2 &= a_1^2 \left(\frac{1}{4} \Lambda_2 R_{21}' - \frac{3}{4} \Lambda_1 R_{12}' + \frac{1}{4} \Lambda_2 R_{23}' \cos \varphi_1 + \frac{1}{4} \Lambda_2 I_{23}' \sin \varphi_1 \right) \\ &+ a_2^2 \left(\frac{1}{4} \Lambda_2 R_{22}' - \frac{3}{4} \Lambda_1 R_{11}' \right) + \frac{3}{4} a_1 a_2 \left(\Lambda_1 I_{13}' \sin \varphi_1 - \Lambda_1 R_{13}' \cos \varphi_1 \right) \\ &- \frac{1}{a_2} f \Lambda_2 \left(\cos \varphi_2 + \bar{\Gamma}_2 \sin \varphi_2 \right) + \sigma \end{aligned} \quad (32)$$

$$\begin{aligned}
D_2 a_2 = f_3 &= -\frac{1}{4} \Lambda_2 I_{21}' a_1^2 a_2 - \frac{1}{4} \Lambda_2 I_{22}' a_2^3 + \frac{1}{4} \Lambda_2 a_1^3 \left(R_{23}' \sin \varphi_1 - I_{23}' \cos \varphi_1 \right) \\
&\quad - \Lambda_2 \bar{\Gamma}_2 f \cos \varphi_2 + \Lambda_2 f \sin \varphi_2 \\
D_2 \varphi_2 = f_4 &= -\frac{1}{4} \Lambda_2 a_1^2 \left(R_{21}' + R_{23}' \cos \varphi_1 + I_{23}' \sin \varphi_1 \right) - \frac{1}{4} \Lambda_2 R_{22}' a_2^2 \\
&\quad + \frac{1}{a_2} \Lambda_2 f \left(\cos \varphi_2 + \bar{\Gamma}_2 \sin \varphi_2 \right) + \tau
\end{aligned} \tag{33}$$

where $R'_{11}, I'_{11}, R'_{12}, I'_{12}, R'_{13}, I'_{13}, R'_{21}, I'_{21}, R'_{22}, I'_{22}$ and R'_{23}, I'_{23} , are all real functions of nonlinear terms. The expressions for them can be found in the Appendix as A6.

We note that here a_{10} can be zero while a_{20} is nonzero or both a_{10} and a_{20} are nonzero.

The results for the case a_{10} is zero are similar to those in Section 3.1. Here, we focus on the condition that both a_{10} and a_{20} are nonzero. We employed the same method to obtain the steady-state motion. Let $D_2 a_1 = D_2 a_2 = 0, D_2 \varphi_1 = D_2 \varphi_2 = 0$, and rearrange the $\sin \varphi_{10}, \cos \varphi_{10}$ and $\sin \varphi_{20}, \cos \varphi_{20}$ as

$$\begin{aligned}
\sin \varphi_{10} &= \frac{3\Lambda_1 a_{20}^2 (R_{11} I_{13} - I_{11} R_{13}) + 3\Lambda_1 a_{10}^2 (R_{12} I_{13} - I_{12} R_{13}) - 4I_{13} (\tau + \sigma)}{3\Lambda_1 a_{10} a_{20} (R_{13}^2 + I_{13}^2)} \\
\cos \varphi_{10} &= \frac{-3\Lambda_1 a_{20}^2 (I_{11} I_{13} + R_{11} R_{13}) - 3\Lambda_1 a_{10}^2 (I_{12} I_{13} + R_{12} R_{13}) + 4R_{13} (\tau + \sigma)}{3\Lambda_1 a_{10} a_{20} (I_{13}^2 + R_{13}^2)} \\
\sin \varphi_{20} &= \frac{\Lambda_2 a_{10}^2 a_{20} (\bar{\Gamma}_2 R_{21} + I_{21}) + \Lambda_2 a_{20}^3 (\bar{\Gamma}_2 R_{22} + I_{22}) - 4\bar{\Gamma}_2 a_{20} \tau}{4\Lambda_2 f (1 + \bar{\Gamma}_2^2)} \\
&\quad + \frac{\Lambda_2 a_{10}^3 (\bar{\Gamma}_2 R_{23} + I_{23}) \cos \varphi_{10} + \Lambda_2 (\bar{\Gamma}_2 I_{23} - R_{23}) a_{10}^3 \sin \varphi_{10}}{4\Lambda_2 f (1 + \bar{\Gamma}_2^2)} \\
\cos \varphi_{20} &= \frac{-\Lambda_2 a_{10}^2 a_{20} (\bar{\Gamma}_2 I_{21} - R_{21}) - \Lambda_2 a_{20}^3 (\bar{\Gamma}_2 I_{22} - R_{22}) - 4a_{20} \tau}{4\Lambda_2 f (1 + \bar{\Gamma}_2^2)} \\
&\quad + \frac{\Lambda_2 a_{10}^3 (\bar{\Gamma}_2 I_{23} - R_{23}) \cos \varphi_{10} + \Lambda_2 a_{10}^3 (\bar{\Gamma}_2 R_{23} - I_{23}) \sin \varphi_{10}}{4\Lambda_2 f (1 + \bar{\Gamma}_2^2)}
\end{aligned} \tag{35}$$

By letting $\sin^2 \varphi_{10} + \cos^2 \varphi_{10} = 1$ and $\sin^2 \varphi_{20} + \cos^2 \varphi_{20} = 1$, these equations are transformed into autonomous equations. The steady-state amplitudes of the response a_{10} and a_{20} are

considered as functions of the solar radiation force f and detuning parameters τ and σ . It is noticed that a_{10} and a_{20} are coupled due to the internal resonance and the solutions are complicated.

We also utilize the nature of the singular points of [Equations \(32\)-\(33\)](#) to determine the stability of the steady-state motion solutions. The Jacobi matrix is

$$A = \begin{bmatrix} a_{11} & a_{12} & a_{13} & a_{14} \\ a_{21} & a_{22} & a_{23} & a_{24} \\ a_{31} & a_{32} & a_{33} & a_{34} \\ a_{41} & a_{42} & a_{43} & a_{44} \end{bmatrix} = \begin{bmatrix} \frac{\partial f_i}{\partial a_1} & \frac{\partial f_i}{\partial a_2} & \frac{\partial f_i}{\partial \varphi_1} & \frac{\partial f_i}{\partial \varphi_2} \end{bmatrix}, \quad (i=1,2,3,4) \quad (36)$$

When the eigenvalues are pure imaginary numbers or have negative real part, the solution is stable. Finally, we can present the stable steady-state solution as

$$\begin{aligned} \xi &= a_{10} \cos \frac{1}{3}(\omega t - \varphi_{10} - \varphi_{20}) + a_{20} \cos(\omega t - \varphi_{20}), \\ \eta &= \Gamma_1 a_{10} \cos \frac{1}{3}(\omega t - \varphi_{10} - \varphi_{20}) + \Gamma_2 a_{20} \cos(\omega t - \varphi_{20}). \end{aligned} \quad (37)$$

It is clear that, although the solar radiation excitation only resonates with the short period motion ($\omega \approx \omega_2$), due to the 1:3 internal resonance, both long period solution and short period solution contribute the final forced resonance solution. In addition, it is found that the nonlinearity and the internal resonance of the system play major roles in adjusting the frequency of the long period solution to exactly one-third of the solar radiation excitation frequency and adjusting the frequency of the short period solution to be the exactly same as frequency of solar radiation excitation. Therefore, the synthesis of the response is still periodic.

4 NUMERICAL SIMULATIONS

In this section, numerical simulations are performed to demonstrate the designing process of two types of novel forced resonance periodic orbits. The frequency-response curve and amplitude of the excitation-amplitude of response curve are obtained with detailed explanations. The possible solution for the steady-state amplitude will be obtained and the corresponding stability is analyzed. Finally, the periodic forced resonance orbits are found.

4.1 CASE I: PRIMARY RESONANCE ORBITS

In this part, we apply the proposed method in Section 3.1 to obtain the stable second primary resonance orbits for the BASs in Table 1. The 283 Emma - S/2003 (283) 1, 22 Kalliope-Linus, and 31 Euphrosyne - S/2019 (31) 1 are randomly chosen from [Table 1](#) as examples.

4.1.1 EXAMPLE: 283 EMMA - S/2003 (283) 1

The (283) Emma and S/2003 (283) 1 binary system is located in the main asteroid belt which rotates around the Sun in a nearly circular orbit with eccentricity as 0.12. Since the shape of (283) Emma is almost a sphere, it is reasonable to consider that the gravitational perturbation due to (283) Emma's shape should be weak. Therefore, this system is suitable to be described by the dynamic model in Section 2. By the orbital data of binary asteroid

systems from Johnston's Archive[45], we obtain its nondimensional planar natural frequencies as $\omega_1= 0.0449$ and $\omega_2= 0.9989$. According to Equation (4), the angular rate of the Sun line in the (283) Emma and S/2003 (283) 1 synodic coordinate system is $\omega=0.9978$.

The plots of a_{20} as a function of τ for different values of solar radiation force f are called frequency-response curves which can be obtained by using Equation (26), as shown in Fig.2. Each point on this curve corresponds to a singular point in a different state plane. We note that although the excitation f is relatively small, the response can be quite large. It is a prototypical property of resonance that small input results in large response due to energy accumulation. As the amplitude of the solar radiation excitation increases, the frequency-response curves bend away from the backbone curve that is shown by a black dotted line in Fig.2.

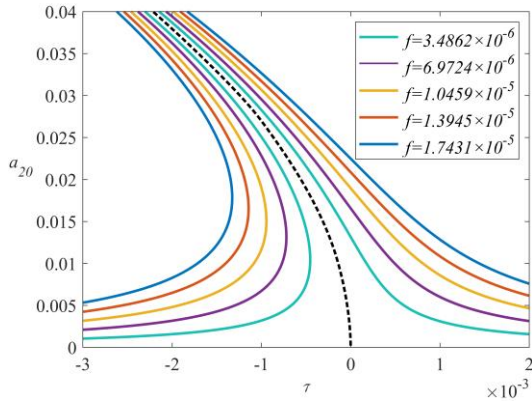


Figure 2 Frequency-response curve of 283 Emma and S/2003 (283) 1

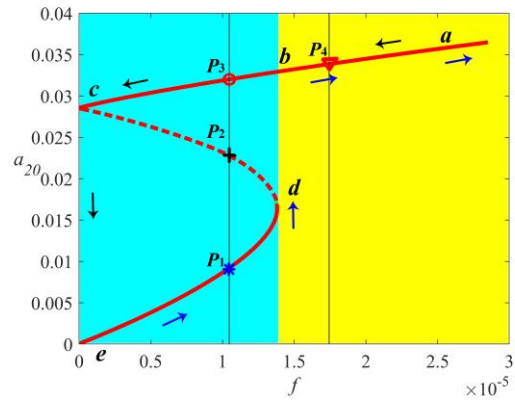


Figure 3 Amplitude of the excitation-amplitude of responds curves of 283 Emma and S/2003 (283) 1 when $\tau=-0.001135$

For the (283) Emma and S/2003 (283) 1 binary system, the detuning parameter is determined as $\tau= \omega-\omega_2=-0.001135$. Based on Equation (26), we also can plot a_{20} as a

function of solar radiation force f for a given $\tau=0.001135$ called as amplitude of the excitation-amplitude of responds curve and shown in Fig.3. Only the solid red line donates stable solutions according to the Equation (28). Let us suppose that f increases, this process is indicated by blue arrows through points e , d , b and a . The jumping phenomenon from point d to point b can be observed along the blue arrow. There are three nontrivial solutions exit if f falls in the cyan region. If f decreases, this process is indicated by black arrows through points a , b , c and e . There is only one stable nontrivial solution until f reaching point b in yellow region. Beyond point b , there are three nontrivial solutions given by Equation (26).

In addition to the complicated nonlinear jumping phenomenon, with different solar radiation forces, the number of nontrivial solution is also different. For example, when the area-to-mass ratio S/M is chosen as $0.003m^2/kg$, corresponding nondimensional solar radiation force f is 1.0458×10^{-5} , the response amplitude of the periodic orbit a_{20} have three values as shown in Fig.3. P_1 ($a_{20}(P_1)=0.009343$) is marked as blue asterisk, P_2 ($a_{20}(P_2)=0.02272$) marked as black cross, and P_3 ($a_{20}(P_3)=0.03206$) is marked as red circle. When the area-to-mass ratio S/M is chosen as $0.005 m^2/kg$ and the corresponding nondimensional solar radiation force f is 1.7431×10^{-5} , the response amplitude of the periodic orbit a_{20} only have one value in Fig.3. P_4 ($a_{20}(P_4)=0.03392$) is marked as red diamond.

Table 2 the values of p and q of different amplitudes

Values	p	q	Stability	Solar Radiation Pressure
$a_{20}(P_1)=0.009343$	0	$q=7.3020\times 10^{-9}$	Stable	$f=1.0458\times 10^{-5}$
$a_{20}(P_2)=0.02272$	0	$q=9.6615\times 10^{-9}$	Stable	$f=1.0458\times 10^{-5}$
$a_{20}(P_3)=0.03206$	0	$q=2.9899\times 10^{-8}$	Stable	$f=1.0458\times 10^{-5}$
$a_{20}(P_4)=0.03392$	0	$q=5.7995\times 10^{-8}$	Stable	$f=1.7431\times 10^{-5}$

Equation (28) is used to evaluate the stability of the nontrivial solutions. Since p and q in Equation (28) are dependent on a_{20} , τ and nonlinear coefficients, the values of p and q can be found in Table 2.

As we concluded, when $p=0$ and q is positive, the corresponding value of state-state amplitudes $a_{20}(P_1)=0.009343$, $a_{20}(P_3)=0.03206$ and $a_{20}(P_4)=0.03392$ are stable. when q is negative, the corresponding value of state-state amplitude $a_{20}(P_2)=0.02272$ is unstable. Similarly, all points in Fig.3 can be evaluated in the same way and all the stable solutions are denoted as solid red line.

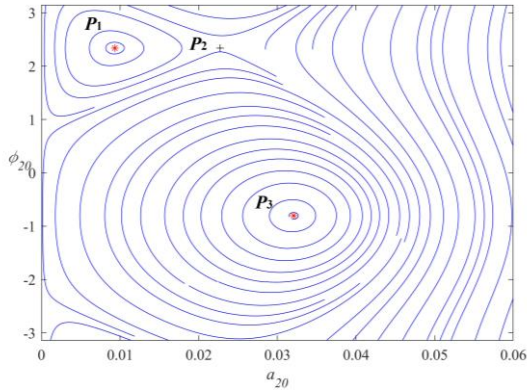


Figure 4(a) State plane portrait when $f=1.0458\times 10^{-5}$

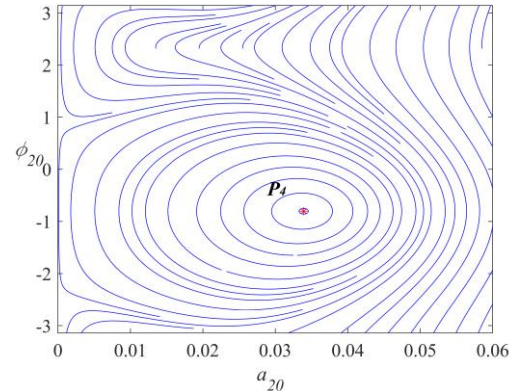


Figure 4(b) State plane portrait when $f=1.7431\times 10^{-5}$

The state plane portrait in Fig.4(a) verify that P_1 and P_3 are center points and P_2 is a

saddle point when $f=1.0458 \times 10^{-5}$. The *state plane portrait* in Fig.4(b) implies that P_4 presents as the only center point when $f=1.7431 \times 10^{-5}$. It is worthy to mention that, with different values of f , based on Fig.3, we always can find the corresponding stable steady-state motion amplitudes a_{20} . The family of the novel forced resonance period orbits can be found.

With the stable solutions for the state-state amplitude a_{20} and phase φ_{20} , we present possible periodic orbits that can be utilized as nominal orbits for practical space missions. Based on Equation (29), we plot the resonance period orbits of the system about different a_{20} in Fig.5. The initial conditions determine which steady-state solution is physically realizable by the system.

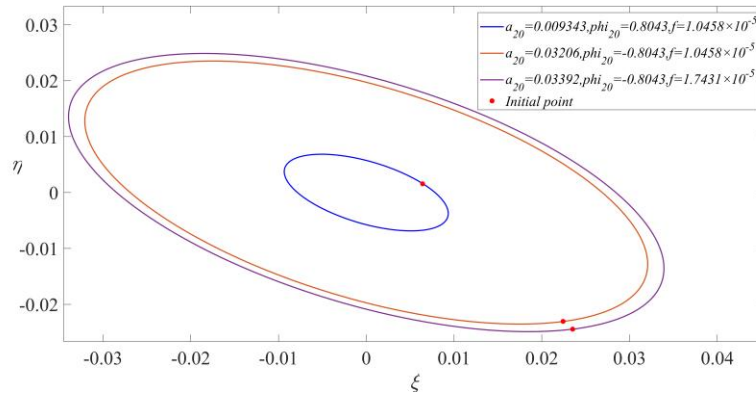


Figure 5 Actual planar trajectory in $L_4\text{-}\zeta\eta\zeta$ with different parameters

4.1.2 EXAMPLE: 22 KALLIOPE AND LINUS

We also apply the proposed method to main belt asteroid binary system 22 Kalliope and Linus which rotates around the Sun in a nearly circular orbit with eccentricity as 0.1.

Based on the orbital data from Johnston's Archive [45], we obtain its nondimensional planar natural frequencies as $\omega_1=0.1821$ and $\omega_2=0.9739$, According to Equation (4), the angular rate of the Sun line in the 22 Kalliope and Linus synodic coordinate system is $\omega=0.9980$.

Fig.6 shows the variation of the frequency-response curves with different values of solar radiation force, which is similar to the frequency-response curves for 283Emma-S/2003 (283) 1.

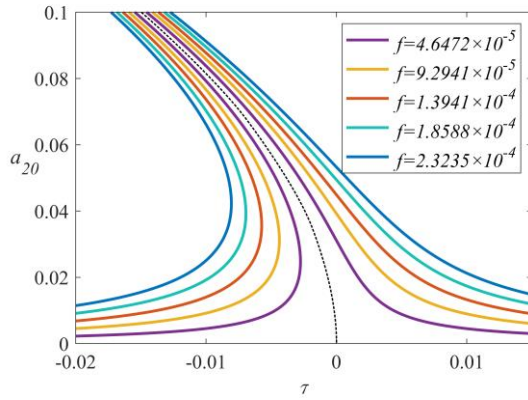


Figure 6 Frequency-response curve of 22 Kalliope and Linus

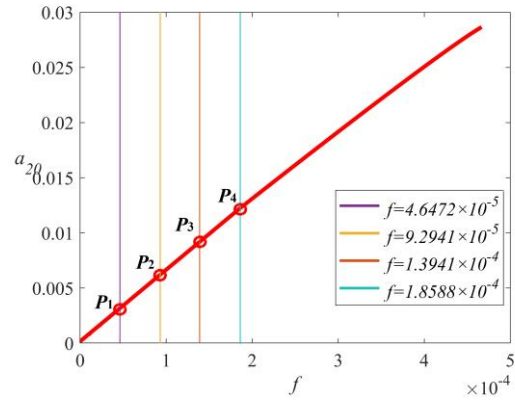


Figure 7 Amplitude of the excitation-amplitude curve of 22 Kalliope and Linus when $\tau=0.01474$

For the 22 Kalliope and Linus system, the detuning number $\tau=\omega-\omega_2=0.01474$, amplitude of the excitation-amplitude of responds curve is plotted in Fig.7. There is no jump phenomenon in such system when the detuning parameter is positive. One given amplitude of the solar radiation force f is corresponding to one amplitude of responding short period motion. When $f=4.6472 \times 10^{-5}$, $f=9.2941 \times 10^{-5}$, $f=1.3941 \times 10^{-4}$, and $f=1.8588 \times 10^{-4}$, the corresponding amplitudes of responses are $a_{20}(P_1)=0.003077$, $a_{20}(P_2)=0.006137$, $a_{20}(P_3)=0.009163$ and $a_{20}(P_4)=0.01214$, respectively, which are all

marked as red circle in Fig.7. Equation (28) is used to evaluate the stability. All points in Fig.7 are evaluated by the Equation (28) and they are all stable. The state plane portrait in Fig.8 verifies the results that P_i ($i=1,2,3,4$) is shown as a center point.

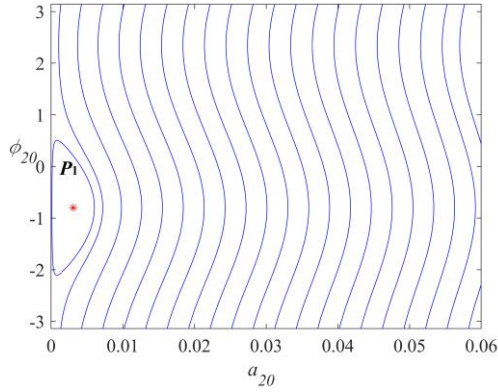


Figure 8(a) State plane portrait when $f=4.6472 \times 10^{-5}$

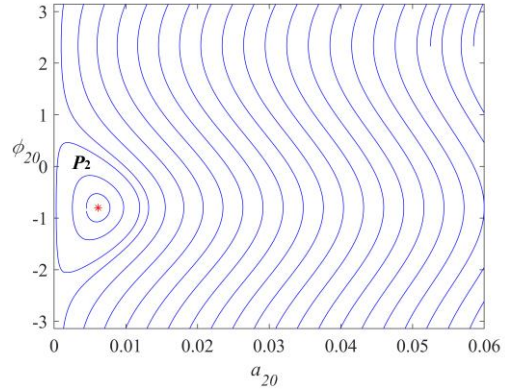


Figure 8 (b) State plane portrait when $f=9.2941 \times 10^{-5}$

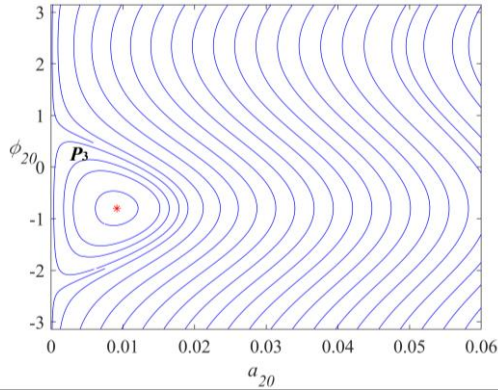


Figure.8(c) State plane portrait when $f=1.3941 \times 10^{-4}$

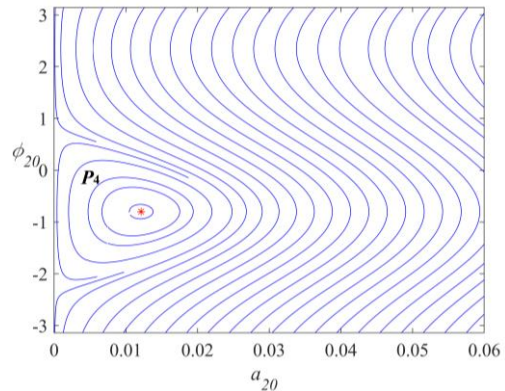


Figure 8(d) State plane portrait when $f=1.8588 \times 10^{-4}$

Fig.9 shows the resonance family with different given magnitudes of solar radiation force f . Starting from the innermost orbit to the outmost one, the S/M increases from 0.02 to $0.08 \text{ m}^2/\text{kg}$, which corresponding to the f varies from 4.6472×10^{-5} to 1.8588×10^{-4} . As solar radiation force f increases, the amplitudes of the resonance periodic motions become larger.

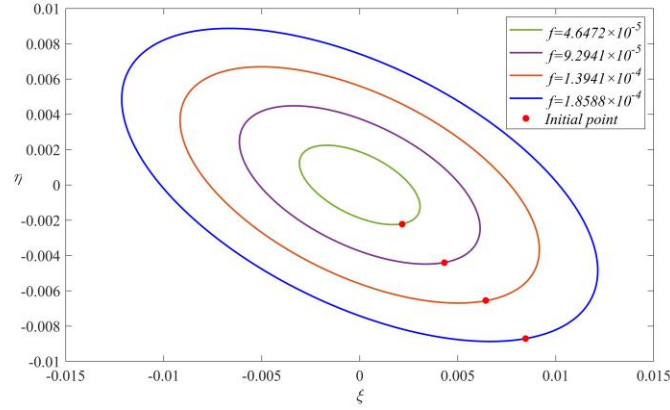


Figure 9 Family of planar trajectories in $L_4\text{-}\xi\eta\zeta$

4.1.3 EXAMPLE: 31 EUPHROSYNE AND S/2019 (31) 1

The 31 Euphrosyne and S/2019 (31) 1 is a main belt asteroid that rotates around the Sun with inclination as 1.4° and eccentricity as 0.043. Based on the orbital data from Johnston's Archive[45], we obtain the system's nondimensional planar natural frequencies as $\omega_1=0.01032$ and $\omega_2=0.9999$. The angular rate of the Sun line in the 31 Euphrosyne and S/2019 (31) 1 synodic coordinate system is $\omega=0.9992$.

Fig.10 shows the variation of the frequency-response curves with different values of solar radiation force. The amplitude of the excitation-amplitude of responds curve when $\tau=\omega-\omega_2=-0.0007139$ is plotted in Fig.11. There is also the jumping phenomenon in such system similar to 283 Emma and S/2003 (283) 1. The two-way jump processes are shown by blue arrows and black arrows. Equation(28) is used to evaluate the stability for all points in Fig.11. The stable amplitudes of a_{20} are denoted as solid line and the unstable amplitudes of a_{20} are denoted as dotted line.

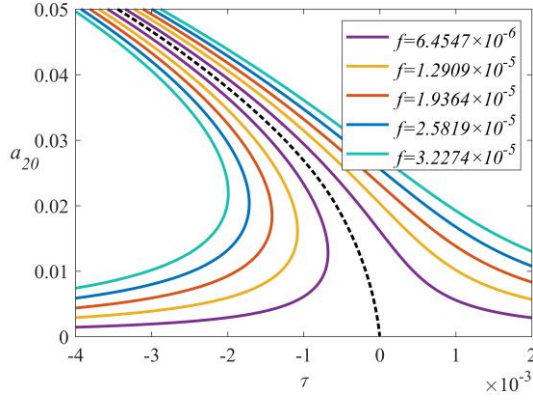


Figure 10 Frequency-response curve of 31 Euphrosyne and S/2019 (31) 1

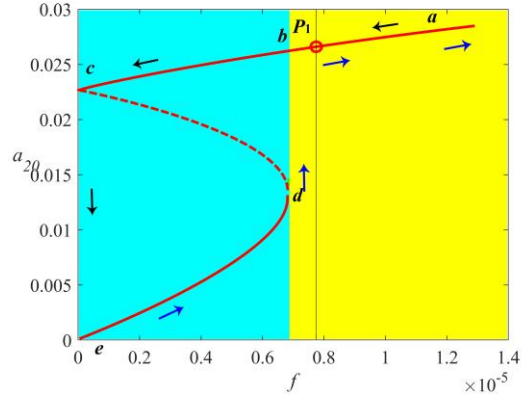


Figure 11 Amplitude of the excitation-amplitude curve of 31 Euphrosyne and S/2019 (31) 1 when $\tau = -0.0007139$

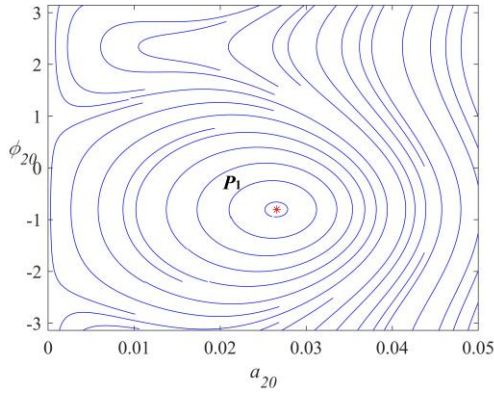


Figure 12 State plane portrait when $f = 7.7456 \times 10^{-6}$

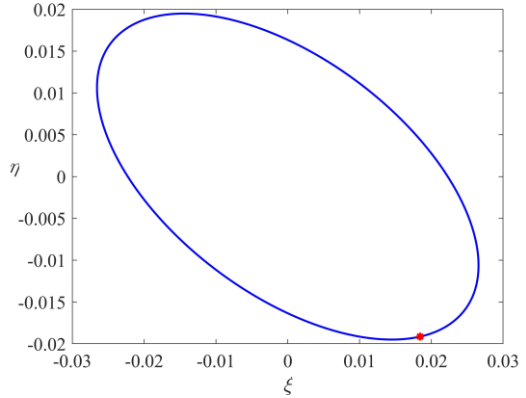


Figure 13 Actual planar trajectories in $L_4 - \xi \eta \zeta$

Particularly, when f equals 7.7456×10^{-6} , the solution $a_{20}(P_1) = 0.02658$ is stable and marked as red circle in Fig.11. The state plane portrait in Fig.12 verifies the results that P_1 is shown as a center points. Fig.13 shows the resonance orbit with given magnitude of solar radiation force f .

It is worthy to mention that the 283 Emma - S/2003 (283) 1, 22 Kalliope - Linus, and 31 Euphrosyne - S/2019 (31) 1 are only taken as examples. The proposed method is suitable for all the systems to find primary resonance orbits.

4.2 CASE II: PRIMARY RESONANCE ORBITS WITH CONSIDERATION OF INTERNAL RESONANCE

In this subsection, we focus on the forced periodic motions with internal resonance. The 2006 Polonskaya, and 4029 Bridges, with nearly ratio $\omega_2/\omega_1=3$ are chosen from [Table 1](#) as examples. The proposed method in Section 3.2 is applied to obtain the stable resonance orbits for those systems. In addition, the energy transferring down from short period motion to long period motion due to the internal resonance will be spotted.

4.2.1 EXAMPLE: 2006 POLONSKAYA-S/2005 (2006) 1

The 2006 Polonskaya-S/2005 (2006) 1 is a main belt binary asteroid system which rotates around the Sun with eccentricity as 0.1933 and inclination as 4.9188° . Based on the orbital data from Johnston's Archive[\[45\]](#), we obtain its nondimensional planar natural frequencies as $\omega_1=0.2750$ and $\omega_2=0.9614$, and the angular rate of the Sun line is $\omega=0.9993$, which suggest the detuning parameters $\tau=\omega-\omega_2=0.0379$, $\sigma=\omega_2-3\omega_1=0.1364$.

Based on the [Equation \(34\)](#) and [Equation \(35\)](#), by letting $\sin^2\varphi_{10}+\cos^2\varphi_{10}=1$ and $\sin^2\varphi_{20}+\cos^2\varphi_{20}=1$, we could obtain the frequency-response equations. The response amplitudes a_{10} and a_{20} are plotted as a function of the amplitude of the solar radiation force f when τ equals 0.03794 and σ equals 0.1364, as shown in [Fig.14](#). The two figures on the left are the enlarged parts of the stable regions of the long- and short-period amplitudes,

respectively. Fig.14 shows how complicated the solutions can be when the short period motion is excited, that is, $\omega \approx \omega_2$.

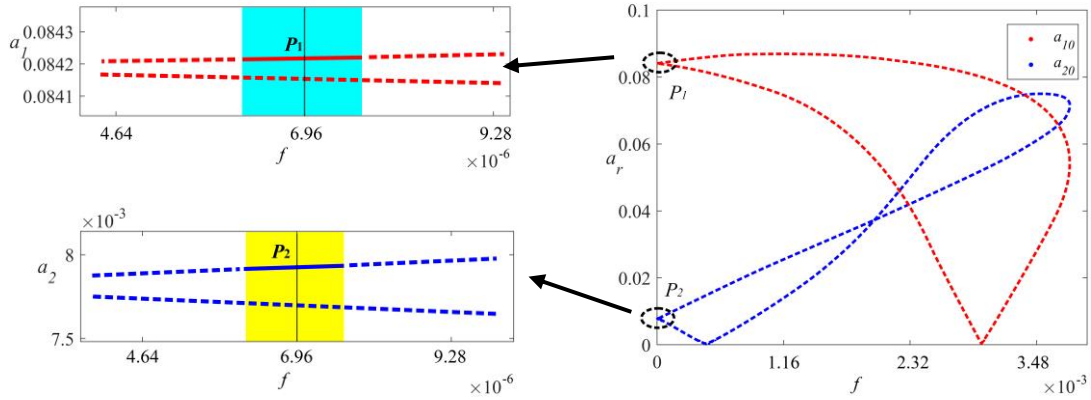


Figure 14 Amplitude of the excitation-amplitude curves of 2006 Polonskaya-S/2005 (2006) 1

The stability of all the steady-state is analyzed by checking the eigenvalues of the Jacobi matrix in Equation (36). The yellow and cyan regions in the enlarged figures highlight the stable ones. It is found, comparing with the simulations in Section 4.1, due to the internal resonance, many portions of these curves correspond to unstable solutions, and hence they cannot be realized in practice.

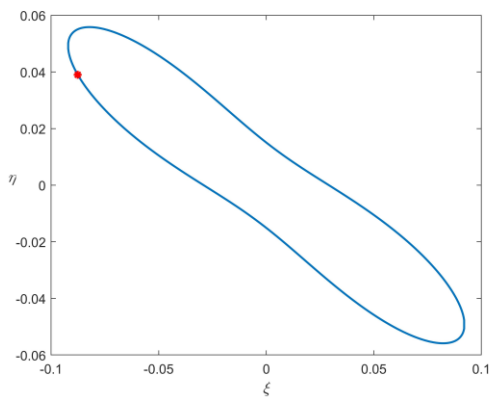


Figure 15(a) Actual planar trajectory in L_4 - $\xi\eta\zeta$

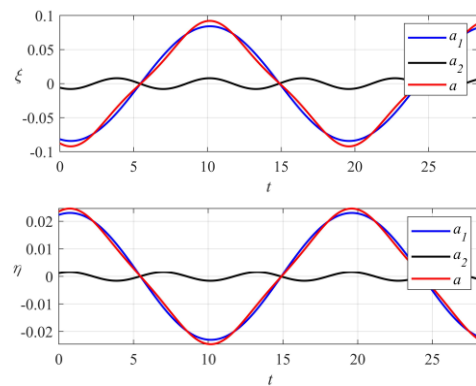


Figure 15(b) Time history diagram for resonance x- and y-motion

We choose $f=6.9598 \times 10^{-6}$ from the stable region in Fig. 14, the stable response amplitudes a_{10} and a_{20} are obtained as 0.08421 and 0.00792, which are marked as P_1 and P_2 in Fig. 14. The corresponding phase φ_{10} , φ_{20} are 0.0336 and 0.7117, respectively. Based on the Equation (37), we plot the periodic motion of the response in Fig.15(a). Fig.15(b) shows the synthesis of the response. In this case, we note that although only the short period motion resonance occurs with the solar radiation excitation, the amplitude of the long period motion can be as much as 10.6 times of the amplitude of the short period motion. This means that the internal resonance provides the mechanism for transferring energy down from short period motion (high mode) to long period motion (low mode). It is also worthy to mention that due to the contribution of nonlinearity, the frequency of the long-period amplitude becomes exactly one-third of the frequency of the short-period amplitude. The family of this type of forced resonance period orbits with consideration of 1:3 internal resonance can be found with different values of f .

4.2.2 EXAMPLE: 4029 BRIDGES- UNNAMED SECONDARY

The 4029 Bridges- unnamed secondary is a near-Earth binary asteroid system, whose orbital eccentricity is 0.1310 and inclination is 5.4370° . Similarly, based on the orbital data from Johnston's Archive[45], we obtain its nondimensional planar natural frequencies $\omega_1=0.3172$ and $\omega_2=0.9483$. The angular rate of the Sun line in the synodic coordinate system is $\omega=0.9995$. The corresponding detuning parameters are $\tau=0.05119$ and $\sigma=-$

0.003304.

The same analysis can be applied to the 4029 Bridges. We plot the amplitude of the excitation-amplitude curves as shown in Fig.16. The two figures on the left are the enlarged parts of the stable region of the long- and short- period amplitude of the excitation-amplitude curves, respectively. The stability of all the steady-state is analyzed by checking the eigenvalues of the Jacobi matrix in Equation (36).

Similar to the results for 2006 Polonskaya, only a few stable solutions exists in this system, which are denoted as solid line in Fig.16. Choosing $f=2.7954 \times 10^{-6}$ from the stable area, we can find $a_{10}(P_1) = 0.04574$, $a_{20}(P_2) = 0.001544$. Based on the Equation (37), we plot the periodic motion to show the synthesis of the response in Fig.17. Due to the internal resonance, the energy from the solar radiation excitation also transfers down from short period motion to long period motion, which is results in large a_{10} and small a_{20} for the finally response.

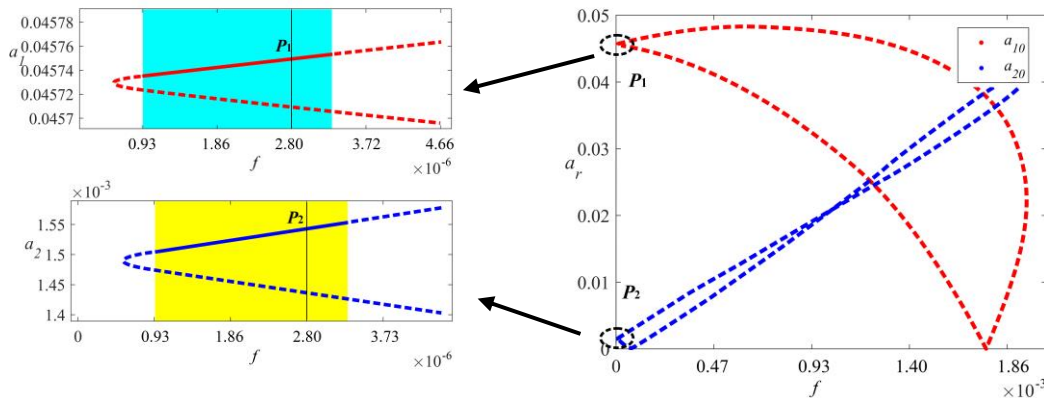


Figure 16 Amplitude of the excitation-amplitude curves of 4029 Bridges- unnamed secondary

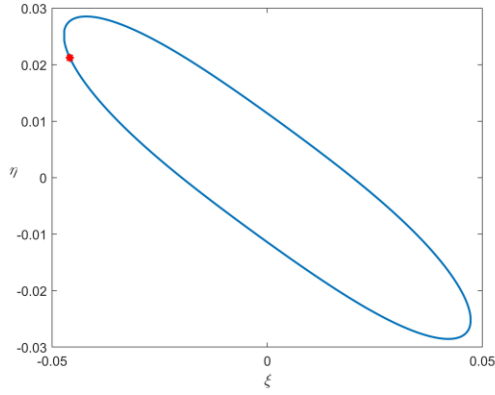


Figure 17(a) Actual planar trajectory in L_4 - $\xi\eta\zeta$

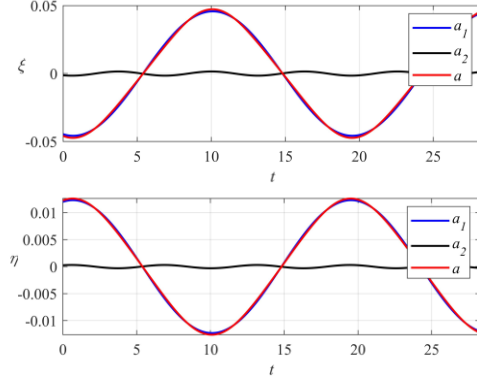


Figure 17(b) Time history diagram for resonance x and y -motion

5 CONCLUSIONS

In this paper, by adopting the CRTBP model for binary asteroid system and taking SRP excitation into account, one novel type of orbits due to primary resonance and one novel type of orbits due to both primary resonance and internal resonance have been found by the method of multiple scales.

Based on the analysis for the natural frequencies of long/short period motion and the frequency for the solar radiation excitation, it is found that the second primary resonance $\omega \approx \omega_2$ is possible phenomena for many binary asteroid systems. In addition, some binary asteroid systems' second natural frequency (short period motion) is around three times of the first natural frequency, that $\omega_2 \approx 3\omega_1$, and the 1:3 internal resonance is also possible for these BASs such as 2006 Polonskaya.

During the investigation for the primary resonance, the frequency-response curves and amplitude of the excitation-amplitude of response curves are obtained, which explain

the evolution of these forced periodic motions in detail. The typical nonlinear phenomena such as multiple solutions and jumping are observed. The stabilities of the steady-states are analyzed by the eigenvalues and the state plane portraits. During the investigation for the primary resonance with consideration of 1:3 internal resonance, the mechanism for internal resonance transferring energy down from short period motion to long period motion is spotted. Due to the nonlinearity and the internal resonance, the frequency of the long-period amplitude becomes exactly one-third of the frequency of the short-period amplitude. The final forced resonance orbits are still periodic.

The current study expands a set of existing periodic solutions for the binary asteroid systems. In addition, the proposed method also can be used to find the forced periodic motions for the single asteroid system in its body-fixed coordinate system.

ACKNOWLEDGMENT

This work is supported in part by the National Natural Science Foundation of China (project no. 11772009), the Beijing Natural Science Foundation (project no. 1192002).

COMPETING FINANCIAL INTERESTS

The authors declare no competing financial interests.

DATA AVAILABILITY

The data that support the plots within this paper and other findings of this study are available from the corresponding author on request.

REFERENCES

- [1] C T Russell, C A Raymond. The Dawn Mission to Vesta and Ceres. *Space Science Reviews*, 163(1), (2011). 3-23. <https://doi.org/10.1007/s11214-011-9836-2>
- [2] D Yeomans, P Antreasian, J-P Barriot, S R Chesley, D Dunham, R Farquhar, B Williams. Radio Science Results During the NEAR-Shoemaker Spacecraft Rendezvous with Eros. *Science (New York, N.Y.)*, 289, (2000). 2085-2088. <https://doi.org/10.1126/science.289.5487.2085>
- [3] M Yoshikawa, A Fujiwara, J Kawaguchi. (2006/08/1). Hayabusa - Its Adventure around the Tiny Asteroid Itokawa.
- [4] B V Sarli, Y Tsuda. Hayabusa 2 extension plan: Asteroid selection and trajectory design. *Acta Astronautica*, 138, (2017). 225-232. <https://doi.org/https://doi.org/10.1016/j.actaastro.2017.05.016>
- [5] J L Margot, M C Nolan, L A M Benner, S J Ostro, R F Jurgens, J D Giorgini, D B Campbell. Binary Asteroids in the Near-Earth Object Population. *Science*. 296(5572), (2002).
- [6] P Pravec, A W Harris. Binary asteroid population - 1. Angular momentum content. *Icarus*, 190(1), (2007). 250-259. <https://doi.org/10.1016/j.icarus.2007.02.023>
- [7] P Helfenstein, J Veverka, P C Thomas, D P Simonelli, K Klaasen, T V Johnson, C Chapman. Galileo photometry of asteroid 243 Ida. *Icarus*, 120(1), (1996). 48-65. <https://doi.org/10.1006/icar.1996.0036>

-
- [8]S Tardivel, P Michel,D J Scheeres.Deployment of a lander on the binary asteroid (175706) 1996 FG3, potential target of the european MarcoPolo-R sample return mission. *Acta Astronautica*, 89, (2013). 60-70. <https://doi.org/10.1016/j.actaastro.2013.03.007>
- [9]A F Cheng, R Michel, M Jutzi, A S Rivkin, A Stickle, O Barnouin, A I M Team.Asteroid Impact & Deflection Assessment mission: Kinetic impactor. *Planetary and Space Science*, 121, (2016). 27-35. <https://doi.org/10.1016/j.pss.2015.12.004>
- [10]H Lei, C Cenci,E Ortore.Secular dynamics around uniformly rotating asteroids. *Monthly Notices of the Royal Astronomical Society*, 485(2), (2019). 2731-2743. <https://doi.org/10.1093/mnras/stz561>
- [11]T Luo,M Xu.Dynamics of the spatial restricted three-body problem stabilized by Hamiltonian structure-preserving control. *Nonlinear Dynamics*, 94(3), (2018). 1889-1905. <https://doi.org/10.1007/s11071-018-4463-z>
- [12]D P Hamilton,J A Burns.Orbital stability zones about asteroids: II. The destabilizing effects of eccentric orbits and of solar radiation. *Icarus*, 96(1), (1992). 43-64. [https://doi.org/10.1016/0019-1035\(92\)90005-R](https://doi.org/10.1016/0019-1035(92)90005-R)
- [13]J Feng,X Y Hou.Secular dynamics around small bodies with solar radiation pressure. *Communications in Nonlinear Science and Numerical Simulation*, 76, (2019). 71-91. <https://doi.org/10.1016/j.cnsns.2019.02.011>
- [14]E M Alessi, G Schettino, A Rossi,G B Valsecchi.Solar radiation pressure resonances in Low Earth Orbits. *Monthly Notices of the Royal Astronomical Society*, 473(2), (2018). 2407-2414. <https://doi.org/10.1093/mnras/stx2507>
- [15]D García Yáñez, D J Scheeres,C R McInnes.On the a and g families of orbits in the Hill problem with solar radiation pressure and their application to asteroid orbiters. *Celestial Mechanics and Dynamical Astronomy*, 121(4), (2015). 365-384. <https://doi.org/10.1007/s10569-015-9604-9>
- [16]T G G Chanut, S Aljbaae, A F B A Prado,V Carruba.Dynamics in the vicinity of (101955) Bennu: solar radiation pressure effects in equatorial orbits. *Monthly Notices of the Royal Astronomical Society*, 470, (2017). 2687-2701. <https://doi.org/10.1093/mnras/stx1204>
- [17]E Morrow, D J Scheeres,D Lubin.Solar Sail Orbit Operations at Asteroids. *Journal of Spacecraft and Rockets*, 38(2), (2001). 279-286. <https://doi.org/10.2514/2.3682>
- [18]X Xin, D J Scheeres,X Hou.Forced periodic motions by solar radiation pressure around uniformly rotating asteroids. *Celestial Mechanics and Dynamical Astronomy*, 126(4), (2016). 405-432. <https://doi.org/10.1007/s10569-016-9701-4>
- [19]S B Broschart,D J Scheeres.Control of Hovering Spacecraft Near Small Bodies: Application to Asteroid 25143 Itokawa. *Journal of Guidance, Control, and Dynamics*, 28(2), (2005). 343-354. <https://doi.org/10.2514/1.3890>
- [20]S Sawai, D J Scheeres,S B Broschart.Control of Hovering Spacecraft Using Altimetry. *Journal of Guidance Control Dynamics*, 25, (2002). 786-795.

<https://doi.org/10.2514/2.4947>

[21]E Mysen,K Aksnes.On the dynamical stability of the Rosetta orbiter. II. *Astronomy & Astrophysics*, 470(3), (2007). 1193-1199. <https://doi.org/10.1051/0004-6361:20077472>

[22]Y Takei, T Saiki, Y Yamamoto, Y Mimasu, H Takeuchi, H Ikeda, Y Tsuda.Hayabusa2's station-keeping operation in the proximity of the asteroid Ryugu. *Astrodynamics*, 4(4), (2020). 349-375. <https://doi.org/10.1007/s42064-020-0083-8>

[23]E Scantamburlo,M Guzzo.Short-period effects of the planetary perturbations on the Sun-Earth Lagrangian point L-3: Planetary perturbations of the Sun-Earth L-3. *Astronomy & Astrophysics*, 638, (2020). <https://doi.org/10.1051/0004-6361/202037696>

[24]Y Oki, Y Tsuda,J i Kawaguchi.Extension of stable terminator orbits around small bodies. *Acta Astronautica*, 157, (2019). 180-188.

<https://doi.org/https://doi.org/10.1016/j.actaastro.2018.12.027>

[25]S B Broschart, G Lantoine,D J Grebow.Quasi-terminator orbits near primitive bodies. *Celestial Mechanics and Dynamical Astronomy*, 120(2), (2014). 195-215.

<https://doi.org/10.1007/s10569-014-9574-3>

[26]D García Yáñez, J-P Sanchez Cuartielles,C R McInnes.Alternating Orbiter Strategy for Asteroid Exploration. *Journal of Guidance, Control, and Dynamics*, 38(2), (2014). 280-291. <https://doi.org/10.2514/1.G000562>

[27]X Y Li, D Qiao,P Li.Frozen orbit design and maintenance with an application to small body exploration. *Aerospace Science and Technology*, 92, (2019). 170-180.

<https://doi.org/10.1016/j.ast.2019.05.062>

[28]K M Roh, H Luehr, M Rothacher,S Y Park.Investigating suitable orbits for the Swarm constellation mission - The frozen orbit. *Aerospace Science and Technology*, 13(1), (2009). 49-58. <https://doi.org/10.1016/j.ast.2008.03.001>

[29]I Jean, A K Misra,A Ng.Solar Radiation Pressure–Compatible Trajectories in the Vicinity of a Binary Asteroid. *Journal of Guidance, Control, and Dynamics*, 42(6), (2019). 1319-1329. <https://doi.org/10.2514/1.G004007>

[30]J Heiligers,D Scheeres.Solar-Sail Orbital Motion About Asteroids and Binary Asteroid Systems. *Journal of Guidance, Control, and Dynamics*, 41, (2018). 1-16.

<https://doi.org/10.2514/1.G003235>

[31]A K de Almeida, A Prado,T Yokoyama.Determination of thrusts to generate artificial equilibrium points in binary systems with applications to a planar solar sail. *Nonlinear Dynamics*, 95(2), (2019). 919-942. <https://doi.org/10.1007/s11071-018-4605-3>

[32]X-Y Hou, X-S Xin,J-L Feng.Forced motions around triangular libration points by solar radiation pressure in a binary asteroid system. *Astrodynamics*, 4(1), (2020). 17-30.

<https://doi.org/10.1007/s42064-019-0060-2>

[33]S Aljbaae, A F B A Prado, D M Sanchez,H Hussmann.Analysis of the orbital stability close to the binary asteroid (90) Antiope. *Monthly Notices of the Royal Astronomical Society*, 496(2), (2020). 1645-1654. <https://doi.org/10.1093/mnras/staa1634>

-
- [34]I Jean, A Ng,A K Misra.Impact of solar radiation pressure modeling on orbital dynamics in the vicinity of binary asteroids. *Acta Astronautica*, 165, (2019). 167-183. <https://doi.org/10.1016/j.actaastro.2019.09.003>
- [35]X Xin, D J Scheeres,X Hou.Forced periodic motions by solar radiation pressure around uniformly rotating asteroids %J *Celestial Mechanics and Dynamical Astronomy*. 126(4), (2016).
- [36]M Hassani, J Roshanian,A M Khoshnood.On-line attitude perturbation estimation in the earth-orbiting satellite. *Aerospace Science and Technology*, 70, (2017). 189-197. <https://doi.org/10.1016/j.ast.2017.07.029>
- [37]F Ferrari,M Lavagna.Periodic motion around libration points in the Elliptic Restricted Three-Body Problem. *Nonlinear Dynamics*, 93(2), (2018). 453-462. <https://doi.org/10.1007/s11071-018-4203-4>
- [38]J F Liu, L Q Chen,N G Cui.Solar sail chaotic pitch dynamics and its control in Earth orbits. *Nonlinear Dynamics*, 90(3), (2017). 1755-1770. <https://doi.org/10.1007/s11071-017-3762-0>
- [39]G Xu,J Xu.On orbital disturbing effects of the solar radiation. *Monthly Notices of the Royal Astronomical Society*, 432(1), (2013). 584-588. <https://doi.org/10.1093/mnras/stt483>
- [40]G Xu,J Xu.On the singularity problem in orbital mechanics. *Monthly Notices of the Royal Astronomical Society*, 429(2), (2013). 1139-1148. <https://doi.org/10.1093/mnras/sts403>
- [41]S Gong,M Macdonald.Review on solar sail technology. *Astrodynamics*, 3(2), (2019). 93-125. <https://doi.org/10.1007/s42064-019-0038-x>
- [42]A H Nayfeh,D T Mook. *Nonlinear Oscillations*. Wiley-VDH verlag GmbH 1995.
- [43]Y J Qian, Z X Liu, X D Yang, I Hwang,W Zhang.Novel Subharmonic Resonance Periodic Orbits of a Solar Sail in Earth-Moon System. *Journal of Guidance Control and Dynamics*, 42(11), (2019). 2532-2540. <https://doi.org/10.2514/1.g004377>
- [44]Y-J Qian, L-Y Yang, X-D Yang,W Zhang.Parametric stability analysis for planar bicircular restricted four-body problem. *Astrodynamics*, 2(2), (2018). 147-159. <https://doi.org/10.1007/s42064-017-0017-2>
- [45]W R Johnston.<http://www.johnstonsarchive.net/astro/astmoons/am-00283.html>.

APPENDIX A: COEFFICIENTS

$$E_i = \frac{x_i - x_o}{\gamma_o}, F_i = \frac{y_i - y_o}{\gamma_o}, D_i^2 = E_i^2 + F_i^2, i=1,2 \quad (\text{A1})$$

$$\begin{aligned} \alpha_{030} &= \sum_{i=1}^2 \frac{\mu_i (35E_i F_i^3 - 15E_i F_i D_i^2)}{2\gamma_o^3 D_i^9}, & \alpha_{120} &= \sum_{i=1}^2 \frac{\mu_i \begin{pmatrix} 105E_i^2 F_i^2 - 15E_i^2 D_i^2 \\ -15F_i^2 D_i^2 + 3D_i^4 \end{pmatrix}}{2\gamma_o^3 D_i^9} \\ \alpha_{210} &= \sum_{i=1}^2 \frac{\mu_i (105E_i^3 F_i - 45E_i F_i D_i^2)}{2\gamma_o^3 D_i^9}, & \alpha_{300} &= \sum_{i=1}^2 \frac{\mu_i (35E_i^4 - 30E_i^2 D_i^2 + 3D_i^4)}{2\gamma_o^3 D_i^9} \\ \beta_{030} &= \sum_{i=1}^2 \frac{\mu_i (35F_i^4 - 30F_i^2 D_i^2 + 3D_i^4)}{2\gamma_o^3 D_i^9}, & \beta_{120} &= \sum_{i=1}^2 \frac{\mu_i (105E_i F_i^3 - 45E_i F_i D_i^2)}{2\gamma_o^3 D_i^9} \\ \beta_{210} &= \sum_{i=1}^2 \frac{\mu_i \begin{pmatrix} 105E_i^2 F_i^2 - 15F_i^2 D_i^2 \\ -15E_i^2 D_i^2 + 3D_i^4 \end{pmatrix}}{2\gamma_o^3 D_i^9}, & \beta_{300} &= \sum_{i=1}^2 \frac{\mu_i (35E_i^3 F_i - 15E_i F_i D_i^2)}{2\gamma_o^3 D_i^9} \end{aligned} \quad (\text{A2})$$

$$\begin{aligned} U_1 &= (3\alpha_{030}\Gamma_1^2\bar{\Gamma}_1 + \alpha_{120}\Gamma_1^2 + 2\alpha_{120}\Gamma_1\bar{\Gamma}_1 + 2\alpha_{210}\Gamma_1 + 3\alpha_{300} + \alpha_{210}\bar{\Gamma}_1) A_1^2 \bar{A}_1 \\ &\quad + \left(6\alpha_{030}\Gamma_1\Gamma_2\bar{\Gamma}_2 + 2\alpha_{120}\Gamma_1\Gamma_2 + 2\alpha_{120}\Gamma_1\bar{\Gamma}_2 + 2\alpha_{120}\Gamma_2\bar{\Gamma}_2 + 2\alpha_{210}\Gamma_1 \right. \\ &\quad \left. + 2\alpha_{210}\Gamma_2 + 6\alpha_{300} + 2\alpha_{210}\bar{\Gamma}_2 \right) A_1 A_2 \bar{A}_2 \\ U_2 &= (3\alpha_{030}\Gamma_2^2\bar{\Gamma}_2 + \alpha_{120}\Gamma_2^2 + 2\alpha_{120}\Gamma_2\bar{\Gamma}_2 + 2\alpha_{210}\Gamma_2 + \alpha_{210}\bar{\Gamma}_2 + 3\alpha_{300}) A_2^2 \bar{A}_2 \\ &\quad + \left(6\alpha_{030}\Gamma_1\Gamma_2\bar{\Gamma}_1 + 2\alpha_{120}\Gamma_1\bar{\Gamma}_1 + 2\alpha_{120}\Gamma_1\Gamma_2 + 2\alpha_{120}\bar{\Gamma}_1\Gamma_2 + 2\alpha_{210}\Gamma_1 \right. \\ &\quad \left. + 2\alpha_{210}\Gamma_2 + 2\alpha_{210}\bar{\Gamma}_1 + 6\alpha_{300} \right) A_1 A_2 \bar{A}_1 \\ V_1 &= (3\beta_{030}\Gamma_1^2\bar{\Gamma}_1 + \beta_{120}\Gamma_1^2 + 2\beta_{120}\Gamma_1\bar{\Gamma}_1 + 2\beta_{210}\Gamma_1 + 3\beta_{300} + \beta_{210}\bar{\Gamma}_1) A_1^2 \bar{A}_1 \\ &\quad + \left(6\beta_{030}\Gamma_1\Gamma_2\bar{\Gamma}_2 + 2\beta_{120}\Gamma_1\Gamma_2 + 2\beta_{120}\Gamma_1\bar{\Gamma}_2 + 2\beta_{120}\Gamma_2\bar{\Gamma}_2 + 2\beta_{210}\Gamma_1 \right. \\ &\quad \left. + 2\beta_{210}\Gamma_2 + 6\beta_{300} + 2\beta_{210}\bar{\Gamma}_2 \right) A_1 A_2 \bar{A}_2 \\ V_2 &= (3\beta_{030}\Gamma_2^2\bar{\Gamma}_2 + \beta_{120}\Gamma_2^2 + 2\beta_{120}\Gamma_2\bar{\Gamma}_2 + 2\beta_{210}\Gamma_2 + \beta_{210}\bar{\Gamma}_2 + 3\beta_{300}) A_2^2 \bar{A}_2 \\ &\quad + \left(6\beta_{030}\Gamma_1\Gamma_2\bar{\Gamma}_1 + 2\beta_{120}\Gamma_1\bar{\Gamma}_1 + 2\beta_{120}\Gamma_1\Gamma_2 + 2\beta_{120}\bar{\Gamma}_1\Gamma_2 + 2\beta_{210}\Gamma_1 \right. \\ &\quad \left. + 2\beta_{210}\Gamma_2 + 2\beta_{210}\bar{\Gamma}_1 + 6\beta_{300} \right) A_1 A_2 \bar{A}_1 \end{aligned} \quad (\text{A3})$$

$$\begin{aligned}
R_{11} + iI_{11} &= \left[\begin{aligned} &6\beta_{030}\Gamma_1\Gamma_2\bar{\Gamma}_1\bar{\Gamma}_2 + 2\beta_{120}\Gamma_1\Gamma_2\bar{\Gamma}_1 + 2\beta_{120}\Gamma_1\bar{\Gamma}_1\bar{\Gamma}_2 + 2\beta_{120}\Gamma_2\bar{\Gamma}_1\bar{\Gamma}_2 + 2\beta_{210}\Gamma_1\bar{\Gamma}_1 \\ &+ 2\beta_{210}\Gamma_2\bar{\Gamma}_1 + 6\beta_{300}\bar{\Gamma}_1 + 2\beta_{210}\bar{\Gamma}_2\bar{\Gamma}_1 + 6\alpha_{030}\Gamma_1\Gamma_2\bar{\Gamma}_2 + 2\alpha_{120}\Gamma_1\Gamma_2 \\ &+ 2\alpha_{120}\Gamma_1\bar{\Gamma}_2 + 2\alpha_{120}\Gamma_2\bar{\Gamma}_2 + 2\alpha_{210}\Gamma_1 + 2\alpha_{210}\Gamma_2 + 6\alpha_{300} + 2\alpha_{210}\bar{\Gamma}_2 \end{aligned} \right] \\
R_{12} + iI_{12} &= \left[\begin{aligned} &3\beta_{030}\Gamma_1^2\bar{\Gamma}_1^2 + \beta_{120}\Gamma_1^2\bar{\Gamma}_1 + 2\beta_{120}\Gamma_1\bar{\Gamma}_1^2 + 2\beta_{210}\Gamma_1\bar{\Gamma}_1 + 3\beta_{300}\bar{\Gamma}_1 + \beta_{210}\bar{\Gamma}_1^2 \\ &+ 3\alpha_{030}\Gamma_1^2\bar{\Gamma}_1 + \alpha_{120}\Gamma_1^2 + 2\alpha_{120}\Gamma_1\bar{\Gamma}_1 + 2\alpha_{210}\Gamma_1 + 3\alpha_{300} + \alpha_{210}\bar{\Gamma}_1 \end{aligned} \right] \\
R_{21} + iI_{21} &= \left[\begin{aligned} &6\beta_{030}\Gamma_1\Gamma_2\bar{\Gamma}_2\bar{\Gamma}_2 + 2\beta_{120}\Gamma_1\Gamma_2\bar{\Gamma}_2 + 2\beta_{120}\Gamma_1\bar{\Gamma}_2\bar{\Gamma}_2 + 2\beta_{120}\Gamma_2\bar{\Gamma}_2\bar{\Gamma}_2 \\ &+ 2\beta_{210}\bar{\Gamma}_2\Gamma_1 + 2\beta_{210}\bar{\Gamma}_2\Gamma_2 + 6\beta_{300}\bar{\Gamma}_2 + 2\beta_{210}\bar{\Gamma}_2\bar{\Gamma}_2 + 6\alpha_{030}\Gamma_1\Gamma_2\bar{\Gamma}_1 \\ &+ 2\alpha_{120}\Gamma_1\bar{\Gamma}_1 + 2\alpha_{120}\Gamma_1\Gamma_2 + 2\alpha_{120}\bar{\Gamma}_1\Gamma_2 + 2\alpha_{210}\Gamma_1 + 2\alpha_{210}\Gamma_2 \\ &+ 2\alpha_{210}\bar{\Gamma}_1 + 6\alpha_{300} \end{aligned} \right] \quad (A4) \\
R_{22} + iI_{22} &= \left[\begin{aligned} &3\beta_{030}\Gamma_2^2\bar{\Gamma}_2^2 + \beta_{120}\Gamma_2^2\bar{\Gamma}_2 + 2\beta_{120}\Gamma_2\bar{\Gamma}_2^2 + 2\beta_{210}\Gamma_2\bar{\Gamma}_2 + 3\beta_{300}\bar{\Gamma}_2 + \beta_{210}\bar{\Gamma}_2^2 \\ &+ 3\alpha_{030}\Gamma_2^2\bar{\Gamma}_2 + \alpha_{120}\Gamma_2^2 + 2\alpha_{120}\Gamma_2\bar{\Gamma}_2 + 2\alpha_{210}\Gamma_2 + \alpha_{210}\bar{\Gamma}_2 + 3\alpha_{300} \end{aligned} \right] \\
U_1' &= \left(3\alpha_{030}\bar{\Gamma}_1^2\Gamma_2 + \alpha_{120}\bar{\Gamma}_1^2 + 2\alpha_{120}\bar{\Gamma}_1\Gamma_2 + \alpha_{210}\Gamma_2 + 2\alpha_{210}\bar{\Gamma}_1 + 3\alpha_{300} \right) \bar{A}_1^2 A_2 e^{i\sigma T_2} \\
&+ \left(3\alpha_{030}\Gamma_1^2\bar{\Gamma}_1 + \alpha_{120}\Gamma_1^2 + 2\alpha_{120}\Gamma_1\bar{\Gamma}_1 + 2\alpha_{210}\Gamma_1 + 3\alpha_{300} + \alpha_{210}\bar{\Gamma}_1 \right) A_1^2 \bar{A}_1 \\
&+ \left(\begin{aligned} &6\alpha_{030}\Gamma_1\Gamma_2\bar{\Gamma}_2 + 2\alpha_{120}\Gamma_1\Gamma_2 + 2\alpha_{120}\Gamma_1\bar{\Gamma}_2 + 2\alpha_{120}\Gamma_2\bar{\Gamma}_2 + 2\alpha_{210}\Gamma_1 \\ &+ 2\alpha_{210}\Gamma_2 + 6\alpha_{300} + 2\alpha_{210}\bar{\Gamma}_2 \end{aligned} \right) A_1 A_2 \bar{A}_2 \\
U_2' &= \left(\alpha_{030}\Gamma_1^3 + \alpha_{120}\Gamma_1^2 + \alpha_{210}\Gamma_1 + \alpha_{300} \right) A_1^3 e^{-i\sigma T_2} \\
&+ \left(3\alpha_{030}\Gamma_2^2\bar{\Gamma}_2 + \alpha_{120}\Gamma_2^2 + 2\alpha_{120}\Gamma_2\bar{\Gamma}_2 + 2\alpha_{210}\Gamma_2 + \alpha_{210}\bar{\Gamma}_2 + 3\alpha_{300} \right) A_2^2 \bar{A}_2 \\
&+ \left(\begin{aligned} &6\alpha_{030}\Gamma_1\Gamma_2\bar{\Gamma}_1 + 2\alpha_{120}\Gamma_1\bar{\Gamma}_1 + 2\alpha_{120}\Gamma_1\Gamma_2 + 2\alpha_{120}\bar{\Gamma}_1\Gamma_2 + 2\alpha_{210}\Gamma_1 \\ &+ 2\alpha_{210}\Gamma_2 + 2\alpha_{210}\bar{\Gamma}_1 + 6\alpha_{300} \end{aligned} \right) A_1 A_2 \bar{A}_1 \\
V_1' &= \left(3\beta_{030}\bar{\Gamma}_1^2\Gamma_2 + \beta_{120}\bar{\Gamma}_1^2 + 2\beta_{120}\bar{\Gamma}_1\Gamma_2 + \beta_{210}\Gamma_2 + 2\beta_{210}\bar{\Gamma}_1 + 3\beta_{300} \right) \bar{A}_1^2 A_2 e^{i\sigma T_2} \\
&+ \left(3\beta_{030}\Gamma_1^2\bar{\Gamma}_1 + \beta_{120}\Gamma_1^2 + 2\beta_{120}\Gamma_1\bar{\Gamma}_1 + 2\beta_{210}\Gamma_1 + 3\beta_{300} + \beta_{210}\bar{\Gamma}_1 \right) A_1^2 \bar{A}_1 \\
&+ \left(\begin{aligned} &6\beta_{030}\Gamma_1\Gamma_2\bar{\Gamma}_2 + 2\beta_{120}\Gamma_1\Gamma_2 + 2\beta_{120}\Gamma_1\bar{\Gamma}_2 + 2\beta_{120}\Gamma_2\bar{\Gamma}_2 + 2\beta_{210}\Gamma_1 \\ &+ 2\beta_{210}\Gamma_2 + 6\beta_{300} + 2\beta_{210}\bar{\Gamma}_2 \end{aligned} \right) A_1 A_2 \bar{A}_2 \\
V_2' &= \left(\beta_{030}\Gamma_1^3 + \beta_{120}\Gamma_1^2 + \beta_{210}\Gamma_1 + \beta_{300} \right) A_1^3 e^{-i\sigma T_2} \\
&+ \left(3\beta_{030}\Gamma_2^2\bar{\Gamma}_2 + \beta_{120}\Gamma_2^2 + 2\beta_{120}\Gamma_2\bar{\Gamma}_2 + 2\beta_{210}\Gamma_2 + \beta_{210}\bar{\Gamma}_2 + 3\beta_{300} \right) A_2^2 \bar{A}_2 \quad (A5) \\
&+ \left(\begin{aligned} &6\beta_{030}\Gamma_1\Gamma_2\bar{\Gamma}_1 + 2\beta_{120}\Gamma_1\bar{\Gamma}_1 + 2\beta_{120}\Gamma_1\Gamma_2 + 2\beta_{120}\bar{\Gamma}_1\Gamma_2 + 2\beta_{210}\Gamma_1 \\ &+ 2\beta_{210}\Gamma_2 + 2\beta_{210}\bar{\Gamma}_1 + 6\beta_{300} \end{aligned} \right) A_1 A_2 \bar{A}_1
\end{aligned}$$

$$\begin{aligned}
R_{11}' + iI_{11}' &= \left[\begin{aligned} &6\beta_{030}\Gamma_1\Gamma_2\bar{\Gamma}_1\bar{\Gamma}_2 + 2\beta_{120}\Gamma_1\Gamma_2\bar{\Gamma}_1 + 2\beta_{120}\Gamma_1\bar{\Gamma}_1\bar{\Gamma}_2 + 2\beta_{120}\Gamma_2\bar{\Gamma}_1\bar{\Gamma}_2 \\ &+ 2\beta_{210}\Gamma_1\bar{\Gamma}_1 + 2\beta_{210}\Gamma_2\bar{\Gamma}_1 + 6\beta_{300}\bar{\Gamma}_1 + 2\beta_{210}\bar{\Gamma}_2\bar{\Gamma}_1 + 6\alpha_{030}\Gamma_1\Gamma_2\bar{\Gamma}_2 \\ &+ 2\alpha_{120}\Gamma_1\Gamma_2 + 2\alpha_{120}\Gamma_1\bar{\Gamma}_2 + 2\alpha_{120}\Gamma_2\bar{\Gamma}_2 + 2\alpha_{210}\Gamma_1 + 2\alpha_{210}\Gamma_2 + 6\alpha_{300} \\ &+ 2\alpha_{210}\bar{\Gamma}_2 \end{aligned} \right] \\
R_{12}' + iI_{12}' &= \left[\begin{aligned} &3\beta_{030}\Gamma_1^2\bar{\Gamma}_1^2 + \beta_{120}\Gamma_1^2\bar{\Gamma}_1 + 2\beta_{120}\Gamma_1\bar{\Gamma}_1^2 + 2\beta_{210}\Gamma_1\bar{\Gamma}_1 + 3\beta_{300}\bar{\Gamma}_1 + \beta_{210}\bar{\Gamma}_1^2 \\ &+ 3\alpha_{030}\Gamma_1^2\bar{\Gamma}_1 + \alpha_{120}\Gamma_1^2 + 2\alpha_{120}\Gamma_1\bar{\Gamma}_1 + 2\alpha_{210}\Gamma_1 + 3\alpha_{300} + \alpha_{210}\bar{\Gamma}_1 \end{aligned} \right] \\
R_{13}' + iI_{13}' &= \left[\begin{aligned} &3\beta_{030}\bar{\Gamma}_1^3\Gamma_2 + \beta_{120}\bar{\Gamma}_1^3 + 2\beta_{120}\bar{\Gamma}_1^2\Gamma_2 + \beta_{210}\bar{\Gamma}_1\Gamma_2 + 2\beta_{210}\bar{\Gamma}_1^2 + 3\beta_{300}\bar{\Gamma}_1 \\ &+ 3\alpha_{030}\bar{\Gamma}_1^2\Gamma_2 + \alpha_{120}\bar{\Gamma}_1^2 + 2\alpha_{120}\bar{\Gamma}_1\Gamma_2 + \alpha_{210}\Gamma_2 + 2\alpha_{210}\bar{\Gamma}_1 + 3\alpha_{300} \end{aligned} \right] \\
R_{21}' + iI_{21}' &= \left[\begin{aligned} &6\beta_{030}\Gamma_1\Gamma_2\bar{\Gamma}_2\bar{\Gamma}_2 + 2\beta_{120}\Gamma_1\Gamma_2\bar{\Gamma}_2 + 2\beta_{120}\Gamma_1\bar{\Gamma}_2\bar{\Gamma}_2 + 2\beta_{120}\Gamma_2\bar{\Gamma}_2\bar{\Gamma}_2 + 6\alpha_{300} \\ &+ 2\beta_{210}\bar{\Gamma}_2\Gamma_1 + 2\beta_{210}\bar{\Gamma}_2\Gamma_2 + 6\beta_{300}\bar{\Gamma}_2 + 2\beta_{210}\bar{\Gamma}_2\bar{\Gamma}_2 + 6\alpha_{030}\Gamma_1\Gamma_2\bar{\Gamma}_1 \\ &+ 2\alpha_{120}\Gamma_1\bar{\Gamma}_1 + 2\alpha_{120}\Gamma_1\Gamma_2 + 2\alpha_{120}\bar{\Gamma}_1\Gamma_2 + 2\alpha_{210}\Gamma_1 + 2\alpha_{210}\Gamma_2 + 2\alpha_{210}\bar{\Gamma}_1 \end{aligned} \right] \\
R_{22}' + iI_{22}' &= \left[\begin{aligned} &3\beta_{030}\Gamma_2^2\bar{\Gamma}_2^2 + \beta_{120}\Gamma_2^2\bar{\Gamma}_2 + 2\beta_{120}\Gamma_2\bar{\Gamma}_2^2 + 2\beta_{210}\Gamma_2\bar{\Gamma}_2 + 3\beta_{300}\bar{\Gamma}_2 + \beta_{210}\bar{\Gamma}_2^2 \\ &+ 3\alpha_{030}\Gamma_2^2\bar{\Gamma}_2 + \alpha_{120}\Gamma_2^2 + 2\alpha_{120}\Gamma_2\bar{\Gamma}_2 + 2\alpha_{210}\Gamma_2 + \alpha_{210}\bar{\Gamma}_2 + 3\alpha_{300} \end{aligned} \right] \\
R_{23}' + iI_{23}' &= \left[\begin{aligned} &\beta_{030}\Gamma_1^3\bar{\Gamma}_2 + \beta_{120}\Gamma_1^2\bar{\Gamma}_2 + \beta_{210}\Gamma_1\bar{\Gamma}_2 + \beta_{300}\bar{\Gamma}_2 + \alpha_{030}\Gamma_1^3 + \alpha_{120}\Gamma_1^2 + \alpha_{210}\Gamma_1 \\ &+ \alpha_{300} \end{aligned} \right] \quad (A6)
\end{aligned}$$